POROUS MEMBRANE-BASED SENSOR DEVICES FOR BIOMOLECULES AND BACTERIA DETECTION

A Dissertation

by

PEI-HSIANG TSOU

Submitted to the Office of Graduate Studies of
Texas A&M University
in partial fulfillment of the requirements for the degree of

DOCTOR OF PHILOSOPHY

August 2012

Major Subject: Electrical Engineering

Porous Membrane-Based Sensor Devices for Biomolecules and Bacteria Detection

POROUS MEMBRANE-BASED SENSOR DEVICES FOR BIOMOLECULES AND BACTERIA DETECTION

A Dissertation

by

PEI-HSIANG TSOU

Submitted to the Office of Graduate Studies of
Texas A&M University
in partial fulfillment of the requirements for the degree of

DOCTOR OF PHILOSOPHY

Approved by:

Chair of Committee,	Jun Kameoka
Committee Members,	Chin B. Su
	Chanan Singh
	Kuang-An Chang
Head of Department,	Costas N. Georghiades

August 2012

Major Subject: Electrical Engineering

ABSTRACT

Porous Membrane-Based Sensor Devices for Biomolecules and Bacteria Detection.

(August 2012)

Pei-Hsiang Tsou, B.S., National Chiao Tung University, Taiwan;

M.S., Texas A&M University

Chair of Advisory Committee: Dr. Jun Kameoka

Biological/biochemistry analyses traditionally require bulky instruments and a great amount of volume of biological/chemical agents, and many procedures have to be performed in certain locations such as medical centers or research institutions. These limitations usually include time delay in testing. The delays may be critical for some aspects such as disease prevention or patient treatment. One solution to this issue is the realization of point-of-care (POC) testings for patients, a domain in public health, meaning that health cares are provided near the sites of patients using well-designed and portable medical devices. Transportation of samples between local and central institutions can therefore be reduced, facilitating early and fast diagnosis. A closely related topic in engineering, lab-on-a-chip (LOC), has been discussed and practiced in recent years. LOC emphasizes integrating several functions of laboratory processes in a small portable device and performing analysis using only a very small amount of sample volume, to achieve low-cost and rapid analysis. From an engineer's point of view, LOC is the strategy to practice the idea of POC testing.

This dissertation aimed at exploring the POC potentials of porous membrane-base LOC devices, which can be used to simplify traditional and standard laboratory procedures. In this study, three LOC prototypes are shown and discussed. First the protein sensor incorporating with silica nanofiber membrane, which has shown 32 times more improvement of sensitivity than a conventional technique and a much shorter detection time; secondly the bacteria filter chip that uses a sandwiched aluminum oxide membrane to stabilize the bacteria and monitor the efficacy of antibiotics, which has reduced the test time from 1 day of the traditional methods to 1 hour; the third is the sensor combining microfluidics and silica nanofiber membrane to realize Surface Enhanced Raman Spectroscopy on bio-molecules, which has enhancement factor 10^9 and detection limit down to nanomolar, but simple manufacturing procedures and reduced fabrication cost. These results show the porous-base membrane LOC devices may have potentials in improving and replacing traditional detection methods and eventually be used in POC applications.

DEDICATION

To my parents and family members.

ACKNOWLEDGEMENTS

I would like to thank my committee chair, Dr. Kameoka, and my committee members: Dr. Su, Dr. Singh, and Dr. Chang, for their guidance and support throughout the course of this research.

I also want to thanks my friends, colleagues for making my life in Texas A&M University an interesting experience. I also want to extend my gratitude to Materials Characterization Facility and Microscopy and Imaging Center, which provided the fabrication and observation instruments.

Finally, thanks to my parent for their encouragement, patience and love.

NOMENCLATURE

AAO	Anodic Aluminum Oxide
CFU	Colony-Forming Unit
ELISA	Enzyme-Linked Immunosorbant Assay
LED	Light-Emitting-Diode
MIC	Minimum Inhibitory Concentration
MPIPC	Methoxyphenylisoxazolylpenicillin
MSSA	Methicillin-Sensitive Staphylococcus Aureus
MRSA	Methicillin-Resistant Staphylococcus Aureus
PBS	Phosphate-Buffered Saline
PDMS	Polydimethylsiloxane
POC	Point-of-Care
PVP	Polyvinylpyrrolidone
SEM	Scanning Electron Microscope
SERS	Surface Enhanced Raman Scattering
SOG	Spin-on-Glass Coating Solution
VAP	Ventilator-Associated Pneumonia
VCM	Vancomycin

TABLE OF CONTENTS

Page

LIST OF FIGURES

Page

Page

Page

LIST OF TABLES

1. INTRODUCTION: POINT-OF-CARE-TESTING AND LAB-ON-A-CHIP

1.1 Point-of-Care-Testing

Healthy living has become an important subject as human's basic urges such as hunger and thirst are gradually satisfied, whether in a convenient city or in a rural countryside. Patients go to clinics or hospitals and look for clinicians' diagnosis when some symptoms have interrupted their daily lives. A typical diagnostic process may involve assessing information from body fluids such as blood, urines, saliva, etc. Clinicians then determine proper treatments for patients based on biological and chemical parameters in these body fluids. A central laboratory is often required to analyze these specimens for the next few hours or days. For example, a blood testing conducted in laboratory based system requires 11 steps, which are: (1) order the test; (2) process the test request; (3) draw blood sample; (4) transport the sample; (5) label and store the sample; (6) centrifuge the sample; (7) sort the serum sample to analyzers; (8) analyze the sample; (9) review the results; (10) report the results to the department; (11) clinicians determine the treatment.[1] For some aspects such as disease prevention or patient treatment, the delays may be critical. To resolve this issue, some clinicians have adapting point-of-care (POC) testing, in which small and portable analytical devices are used near patients' sites to monitor their health conditions. The operator of the POC testing device can be patients themselves, or proper trained persons, depending on situations of patients' health status.

This dissertation follows the style of *Lab on a Chip.*

The abovementioned blood testing example, if conducted with a POC system, may take only 5 steps: (1) order the test; (2) draw blood sample; (3) analyze the sample; (4) review the result; (5) clinicians determine the treatment.[1] The steps that the sample has to be transported to the central lab, analyzed, and reported back to the department are simplified by using the POC system to perform rapid but reliable analysis of the sample. Currently POC testing devices have been performed in several situations: bedside glucose testing, urine pregnancy testing, infectious disease testing, fecal occult blood testing, dipstick urinalysis, probing the information of blood gases and electrolytes, coagulation, cardiac markers, Hemoglobin A1c, and intraoperative parathyroid hormone, and physician-performed microscopy.[2] Optimal POC test device might require characteristics such as: results are strong correlated to those from standard laboratory procedures, minimum variability in test results, easy interpretation and rapid availability of test results, rapid availability of test results, portability of testing equipment, low maintenance, minimal or no use of blood, minimal cost, fool-proof testing methodology, stability of test equipment in various different environments, long shelf lives of reagents, and well quality control. POC test device also have to be developed and tested under the government's regulations, which usually require manufacturers to provide solid scientific evidences to show both safety and efficacy of the devices.[1,3]

1.2 Lab-on-a-Chip

Some of the requirements of POC testing devices are interestingly coincide with the features of lab-on-a-chip (LOC) concepts from an engineer's point of view. LOC

devices emphasize biological, physical, and/or chemical testing on a small portable device that has one or a few laboratory functions, and focus on handling relative smaller volumes of analytes, fluid down to picoliter scale, than conventional laboratory procedures to achieve low cost and rapid analysis. The LOC device is categorized as a subset of microelectromechanical systems (MEMS), which utilizes the matured semiconductor device fabrication technologies, such as thin film deposition, photolithography, and etching to create small electro/mechanical devices with component size ranging from 1 to 100 μm. The development of LOC devices can be dated back to Stephen C. Terry's gas chromatograph article published in 1979.[4] In the paper, he described a system including a sample injection valve, a capillary column, and a thermal conductivity detector that were fabricated on a same silicon substrate. The use of photolithography and chemical etching techniques reduced the size 3 orders of magnitude compared to traditional bulky instruments. The progresses of fabricating channels, pumps, mixers, valves, and fluidic control structures on substrate during the following decades have further improved the development of LOC devices. The first commercialized LOC product was claimed by Agilent Technologies for the company's 2100 Bioanalyzer in 1999.[5] This LOC system consisted a glass-based microfluidic chip with 16 sample wells and inter-connected channel networks, and a computer system with signal reader and analyzer to perform electrophoretic or flow cytometric assay. The substrates used for LOC devices can be silicon, glass, or polymers, such as elastomer polydimethylsiloxane (PDMS), thermoplastic polymethylmethacrylate (PMMA), polycarbonate (PC), cyclic olefin copolymer (COC), polysulfone (PSU), polypropylene

(PP), polyethylene (PE), polyoxymethylene (POM), liquid crystal polymer (LCP), and polyether ether ketone (PEEK). Photolithography is still widely used for fabricating silicon and glass-based LOC devices. For polymeric materials, the fabrication methods of polymeric LOC devices can be molding, hot/cold embossing, injection molding, thermoforming, laser ablation, and micromilling. The fabrication methods of LOC devices are briefly described as follows:

(1) Photolithography: Typically fabricated on silicon and/or silica based substrates, the procedures involve using photoresist, photomask, and UV to define the 2D pattern on the substrates, followed by physical or chemical etching process to create 3D structures.

(2) Laser ablation: Laser ablation creates fine features by concentrating laser energy on a small spot with a few μm in diameter to evaporate or sublimate unwanted part of target material.[6-9]

(3) Micromilling: Similar to traditional milling, micromilling can create small structures in μm scale on metals and polymers using cutter with dimension as small as 10 μm in diameter.[10-12]

(4) Replica molding: The liquid bulk polymer/curing agent mixture is poured on a mold and solidified after polymerization and cross-linking.[13-16]

(5) Injection molding: The polymer granulate is heated to melt and injected into the cavity of a mold. Specific structure is then formed after the molten polymer cools and hardens.[17-20]

(6) Hot embossing: The polymer foil is placed on mold and heated to melt. A substrate plate with rough surface vertically presses the melt into the mold. After the molten polymer cools to demolding temperature, it is separated from the mold by raising the substrate plate. Hot embossing is featured by the residue layer of polymer that is adhered on the rough surface of the substrate place. It helps to remove the structured polymer from the mold during the demolding process.[21-23]

(7) Thermoforming: Thermoforming heats a polymer sheet to the temperature so that the solid sheet can be pressed into the mold and plied to a specific 3D structure. The minimum size of feature depends on the pattern of the mold.[24-27]

Polymer LOC devices are featured by significant lower material cost than silicon and glass. However, different strategies have to be adapted to drive sample fluid into the devices made of different material. The propulsive force of sample fluid can be classified into 5 major categories of methods: capillary-, pressure-, centrifugal-, electrokinetic-, and acoustic-driven flows:[28]

(1) Capillary: Liquid is moved by the capillary forces. The material of LOC substrate may be hydrophilic such as glass or nitro-cellulose, and the movement can be controlled by the wettability and the feature size of porous structure of substrate.[29-32]

(2) Pressure: Pressure driven flow is the most commonly used method in LOC devices. External pressure source such as syringes, micropumps, vacuum pumps, or devices that can create pressure gradients are used to drive the liquid movement in a channel or porous material. Pumping rate and pressure difference between inlet and outlet directly affect the flow speed of the liquid. In some applications when additional

control-channel layers are used, the liquid movement is controlled by the frequency of squeeze and release of the control channels. Pressure driven LOC devices have achieved a certain degree of large scale integration by adapting elastomer as LOC substrate and the peristaltic actuation of the control-channel layers.[33-36]

(3) Centrifugal: Liquid is moved by the centrifugal force, which acts on the liquid along radial outward direction in a channel on a rotating disk. Liquid movement is affected by parameters such as central fugal force, Euler force, Coriolis force, and capillary force.[37-41]

(4) Electrokinetic: Definitions of electrokinetic phenomena cover several effects such as electroosmosis, electrophoresis, and dielectrophoresis. But when the bulk liquid movement in a LOC device is emphasized, the "electrokinetic" usually means electroosmosis. The motion of liquid in the channel is induced by the interaction between the surface charges of the channel wall and the electric field applied at the both ends of the channel. The feature of electrokinetic driven LOC devices is simplicity compared to others. The anode and cathode side of the applied electric field, and the polarity of surface charges decide the direction of the flow. Electrowetting driven flow is also defined in this category. The sample and reagent move in the form of individual droplets. The movement of droplet is steered by the electrode array embedded under an insulated and hydrophobic layer. It is featured by programmable movement with a control electronic instrument.[42-45]

(5) Acoustic: The droplet on a hydrophobic surface in air is moved by the surface acoustic waves induced by a piezoelectric transducer.[46-49]

Each of these transportation methods may not be applied to all materials, and the material properties of reagents and substrates may affect the movement of the liquids. For example, capillary driven flow of water-based sample may be applied to glass-based LOC devices, but not for hydrophobic polymer-based LOC devices. On the other hand, electrowetting may transport water droplet much better on hydrophobic surface than hydrophilic glass surface of LOC devices. In summary, the advantages of LOC devices are often describe as: low consumption of sample and reagent fluids, short analysis time, fast heat generation and dissipation, high surface to volume, ratios, integration of several functions, high throughput, low fabrication cost per device in mass production, and etc. studies because of integration of functionality, smaller fluid volumes and stored energies. These advantages, as abovementioned, may aide the development of POC in the future. It is worth noted that in most cases the instruments of measurement are not considered in the integration of the LOC devices, partially because of the limitation of current technologies. Table 1 shows a simplified comparison of the suitability of several expected LOC features for various transport methods of sample/reagent fluids.[28]

Table 1. Suitability of LOC features for different transport methods.

Transport Method	LOC Features						
	Portability	Throughput	Low cost instrument	Low disposable cost	Low volume consumption	High precision	Program-mability
	(Degree of suitability: oo: good; o: average; x: low.)						
Conventional	x	oo	x	oo	o	oo	oo
Capillary	oo	o	oo	oo	o	x	x
Pressure	o	o	oo	o	x	o	o
Pressure w/ large scale integration	o	oo	o	x	oo	oo	oo
Centrifugal	o	o	o	o	o	oo	x
Electrokinetic	o	o	o	o	o	oo	o
Electrowetting	oo	o	o	x	o	oo	oo
Acoustic	oo	o	o	x	o	o	oo

2. ELECTROSPUN MEMBRANE FILTER DEVICE FOR BIOMOLECULAR DETECTION

2.1 Introduction

The background knowledge of two subjects is introduced: electrospinning and ELISA. The electrospinning is the technique used for fabricating the detection medium, a porous membrane that is composed of long nanofibers, similar to a nonwoven fabric. Therefore the terms "membrane" and "fiber mat" are used interchangeably in the texts. ELISA is the acronym of Enzyme-linked immunosorbent assay, which is a matured biochemistry assay able to quantify the amount of molecule in a sample solution. It is the reference method to be compared with by this new membrane-base assay.

2.1.1 Electrospinning

Electrospinning is a way to produce polymer fibers with diameters from several micrometer to tens of nanometer. Its history can date back to Anton Formhals' patent in 1934. The core of this technique is to charge polymer solution with high voltage until ejection. The polymer solution jets then solidify because of solvent evaporation or cooler environment in the air. The choices of polymer are diverse, such as polyethylene oxide (PEO), nylon, polyvinyl alcohol (PVA), polyurethane (PU), liquid crystal like polyphenylene, polyaniline, and natural material such as silk from silkworms or spiders, DNA, etc.[50-64] Metal or semiconductor oxide fibers can also be electrospun by adding oxide precursors to the polymer solutions and removing the polymer parts by calcination.

[65-67] The features of the fibers made from electrospinning are their continuity and small diameter. The nonwoven fiber mats are therefore highly porous with extremely high surface-to-volume ratio. In some application such as biomedical scaffolds, catalysts, or sensors, this high surface-to-volume ratio can improve efficiency of recovery or reduce reaction time.

The components for elctrospinning generally include the polymer solution with a syringe/needle, a mechanical pump, a high voltage power supply, and an electrical grounded fiber collector. The characteristic of polymer solution may affect the final form of fiber. For example, if the solution has lower viscosity, the jets tend to form short and thin fibers, or even from droplets instead of fibers. Basic controllable parameters in electrospinning include electric field (kV/cm) between the nozzle and the collector, flow rate (μL/min), the supply rate of the solution, deposition distance (cm), the distance between the needle tip and the collector, concentration of polymer or other ingredients, and type of collector.

Electrospinning has been found useful in several fields such as modifying mechanical, electrical, optical properties, sensor, filtration, biomedicine, etc. For example, electrospun nylon fibers were incorporated into bulk epoxy resin to increase the stiffness and mechanical strength of the material; electrospun polyaniline/PEO fibers less than 100 nm were found diameter-dependent conductivities; uniaxially aligned polyvinylpyrrolidone (PVP) electrospun fibers can alter light polarization; heat depolymerizable polycarbonate nanofibers were used as sacrificial templates to produce nanofluidic channels; electrospun polyaniline/poly-(ethylene oxide) (PANI/PEO)

nanowire sensors can detect ammonia gas at very low concentration; electrospun membranes have been used as filters to separate aerosol, electrospun poly(e-caprolactone) (PCL) fiber membranes were used as biomedical scaffolds to improve tissue growth; electrospun poly(vinyl alcohol) fiber membranes can supports enzymes and control the release rate.[68-72]

2.1.2 Enzyme-Linked Immunosorbent Assay (ELISA)

The detection of antigen or antibody amount is crucial in medical science. For example, antibodies in human bodies are released by B-cells when B-cells sense antigens such as bacteria or virus. Although various kinds of antibodies are produced, each kind of antibody only recognizes specific receptors on the surface of antigens. The recognition may rely on correct fitting of shape and size of antibody/antigen. Immune defense is triggered once a certain kind of antibodies is binding to the receptors, and T-cells then come to destroy the antigen. Therefore, the presence of certain antibodies implies the existence of the antigens of some known diseases in blood.

Enzyme-Linked Immunosorbant Assay (ELISA) is a common assay used in biochemistry for quantifying target antigen or antibody amount, basing on the fact that an antigen and its corresponding antibody can form a protein complex when they interact. ELISA is typically practiced in a 96-well or 384-well polystyrene plate. For example, a typical procedures of "sandwich ELISA" can be described as:

(1) Antigen/antibody coating: a solution of antigen (to detect antibody) or antibody (to detect antigen) for catching target protein is dispensed in to a well of ELISA plate.

The antigens or antibodies in solution can be adsorbed on the surface by Van der Waals force as they diffuse to the surface.

(2) Blocking agent coating: a solution of non-reacting protein, or blocking agent, is added into the well after removing the antigen or antibody solution. The purpose is to block unoccupied sites, where no antigen or antibody is attached, to prevent unwanted nonspecific binding of other molecules in later steps.

(3) Sample adding and incubation: A sample with target protein (antibody or antigen) is added after removing the blocking agent. The plate is left for 15 minutes of incubation to make antigen and antibody fully react.

(4) Wash: The well is washed 3 to 6 times by buffer solution to remove excess proteins that have not been bound.

(5) Enzyme-linked antibody adding: The secondary antibodies that are linked with detection enzymes horseradish peroxidase (HRP) and able to recognize target protein are applied into the well after wash. The plate is left for 15 minutes of incubation to make target protein and enzyme-linked antibody fully react. The HRP is an enzyme for catalyzing the color change of substrate (a detection reagent) in later step.

(6) Wash: The well is washed 3 to 6 times by buffer solution to remove excess proteins that have not been bound.

(7) HRP-substrate adding: The HRP-substrate is added into the well after wash. The plate is left for 15 minutes before measurement. The HRP enzyme on the secondary antibody, acting as an amplifier, can keep catalyzing the substrate to change the color of HRP-substrate. The degree of color change caused by the concentration of color product

can be measured using an ELISA reader to assess the optical density value of the sample. The amount of target protein can therefore be estimated by comparing the measured value with a standard curve, typically from a serial dilution of target protein solution with known concentration.

Many types of ELISA-like protocols have been created and they can be practiced on various kinds of surfaces, not limited to the ELISA plate. The detection relies on adsorption of the pre-coated antigens or antibodies on the surface for catching the target protein, and the diffusion of antigen and antibody. To improve catching ability, one can either raise the protein concentration or increase coating/incubation time. However, because the size of protein is extremely small compared to the volume of single well, most proteins are washed away before diffusing to the proximity of the well surface and being adsorbed. The condition worsens in lower concentration since very few proteins can attach to the surface. In other word, ELISA's detection ability is limited by the solid surface. A clinical report pointed out ELISA's poor efficiency of the hybridization resulted in low sensitivity and selectivity.[73]

The features of electrospun fiber mat may improve ELISA's detection limit. Similar assay can be practiced in the fiber mat's filter-like structure. This kind of modification may provide at least two advantages. First, the fiber mat has extremely large surface area that can adsorb much more "catcher" protein and provide more exposure area to the sample. Second, the sample is essentially forced to pass the porous structure, and fewer proteins will be wasted. The above idea is practiced in the experimental part. In this subtopic, electrospun PVP/silica fibers mats were studied,

including fabrication conditions versus resultant fibers, and the improved biochemistry sensing ability in ELISA using calcined silica fiber mats. The water soluble PVP was chosen because no toxic solvent was required for the fabrication.

2.2 Experimental

The fabrication processes of electrospun PVP/silica fiber mat are introduced here. A detection assembly with electrospun silica fiber mat is explained as well as its performances.

2.2.1 Fabrication of Electrospun Fiber Mat

The chemicals used for electrospinning were mainly PVP (MW=1 300 000, Aldrich), Spin-on-Glass Coating (SOG) Solution (IC1-200, Futurrex, Inc.), and butanol (Solvent Diluent SD4, Futurrex, Inc.). The SOG was essentially a silica source, as it has been known that proteins tend to be adsorbed on silica surface.

The 80% SOG solution was prepared by diluting original SOG with butanol. The polymer solution for electrospinning was prepared by adding 0.32 g of PVP into 8 ml of the 80% SOG solution so that the PVP concentration was 0.04 g/ml. These parameters were chosen because they provided relative stable conditions for fabricating thinnest electrospun fibers. The mixture was magnetically stirred for 12 hours and then loaded into the syringe with 24 gauge stainless steel needle. The distance between grounded collector and needle was kept 5 cm; the pump rate was set to 8 μL/min; the voltage of power supply was set to 7 kV. A 2 cm-by-2 cm iron mesh was loosely attached on the

collector for receiving the fiber and for facilitating transportation. After 5 minutes of electrospinning, the fiber mat was transferred to a furnace (Isotemp Muffle Furnace 550, Fisher Scientific) and calcined at 500 °C for 12 hours. After the calcination, the PVP was removed and the composition of electrospun fiber mat was solely silica. The fiber mats were fabricated using the above parameters because they resulted in stable and uniform fiber mat with consistent dimension.

2.2.2 ELISA Using Electrospun Fiber Mat

The chemicals used for these modified ELISA tests were bovine serum albumin (BSA) as blocking agent, monoclonal mouse anti-FLAG M2 antibody (Sigma) and monoclonal mouse anti-c-Myc antibody (Sigma) as primary antibodies, goat anti-mouse HRP (Jackson ImmunoResearch Laboratories) and donkey anti-goat HRP (Jackson ImmunoResearch Laboratories) as secondary antibodies. The electrospun fiber mats were fabricated by procedures described in the previous section.

The concept of using electrospun silica fiber mats to improve conventional ELISA detection was tested by following methodology. First, a primary antibody was coated on the fiber mat, followed by blocking agent coating. The primary antibody acted as an active site for capturing target protein. Second, a secondary antibody conjugated with enzyme was applied to the fiber mat, which simulated the application of target molecule. If the primary and secondary antibody matched each other, they formed a stable bonding and remained on the fiber mat after wash. Thirdly, a substrate was then

applied and emitted light signals that was catalyzed by the enzyme on the secondary antibody. The strength of signals also reflected the concentration of target molecule.

2.2.2.1 Non-Specific Binding of Protein on Electrospun Silica Fiber Mat

Although it is known that proteins can be well adsorbed on glass surface, it is uncertain if they can be adsorbed on the surface of electrospun silica fiber mats. Therefore, a non-specific protein binding test was conducted on those fiber mats. A functional protein (primary antibody) and a non-functional protein (BSA) were applied to the fiber mats respectively as the first layer. The results should directly reflect the choice of this first layer if the binding is "non-specific". Detail procedures are described as follows (Figure 1):

(1) Two fiber mats were placed on a glass slide. One of the fiber mats was coated with 10 μl of BSA (1 μg/μl) as the negative control (protein A). The other fiber mat was coated with 10 μl of primary antibody (protein B) monoclonal mouse anti-FLAG M2 (1 μg/μl) and incubated overnight.

(2) Blocking agents were applied to both fiber mat and incubated at room temperature for 30 minutes, followed by 5 minutes of wash with Tween 20/phosphate-buffered saline (PBS) for 5 minutes.

(3) The target protein, simulated using Goat anti-mouse HRP (protein C), was applied to both fiber mats and incubated at room temperature for 30 minutes.

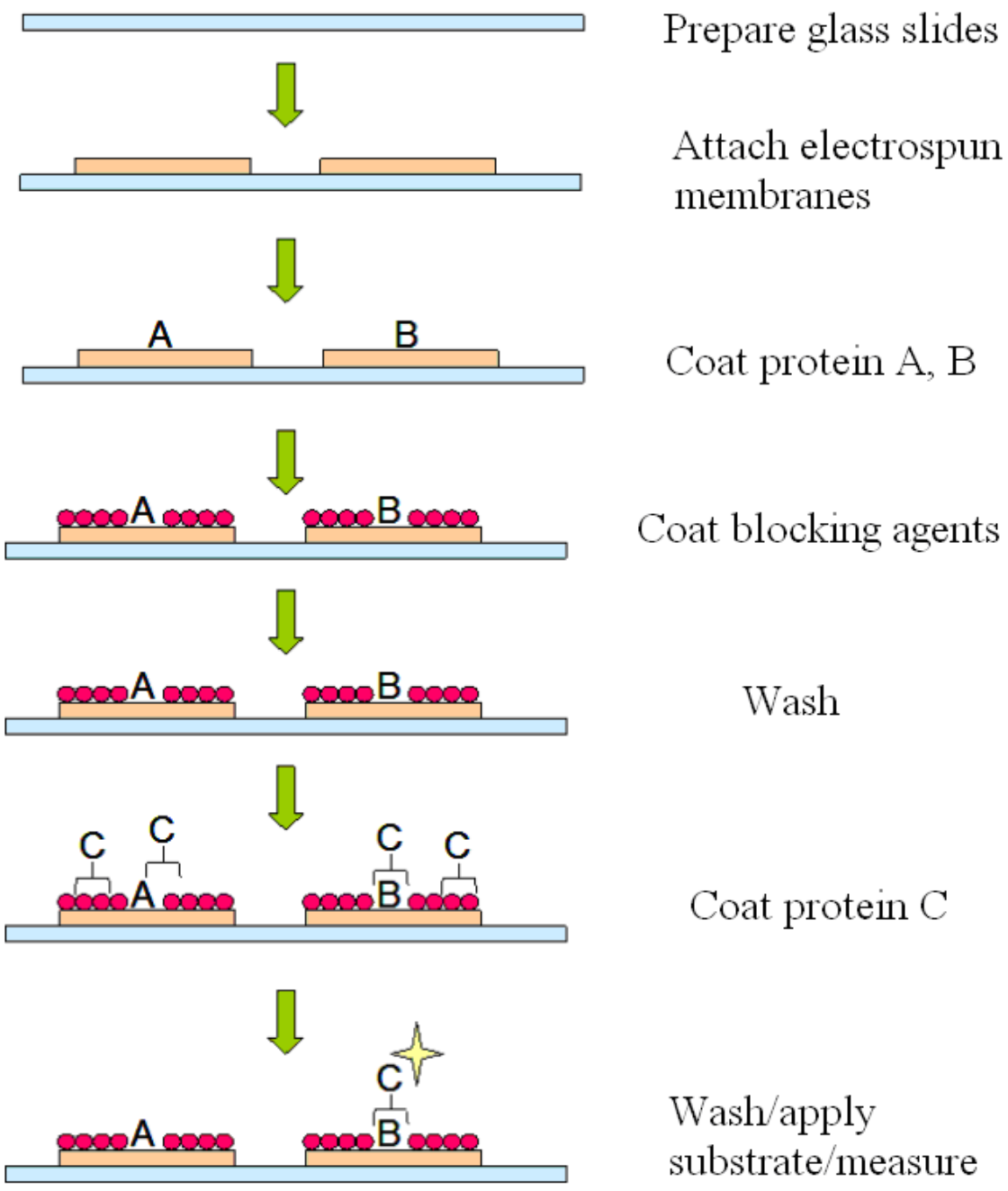

Figure 1. Procedure for the protein-attachment test for electrospun silica nanofiber membranes. Proteins A, B, and C denote BSA, monoclonal mouse anti-FLAG M2 antibody, and goat anti-mouse HRP.

(4) Both fiber mats were washed using Tween 20/PBS 4 times, 10 minutes each time, at room temperature.

(5) Substrates were then applied to both membranes. The results were recorded on x-ray films for 10 seconds and 2 minutes.

2.2.2.2 Specific-Binding of Primary and Secondary Antibody

The experiment in the previous section was to confirm that the proteins (primary antibody and BSA) could non-specifically attach to the surface of electrospun silica fiber mat, which lead to a new ELISA device integrating the fiber mat to investigate the efficiency of protein detection. (Figure 2) This device was connected to a vacuum source to drive the solution through the multi-layer structure. The functions of each layer were described as follow:

(1) stainless steel mesh: to reduce the impact on contact and protect the fiber mat.

(2) electrospun silica fiber mat: to adsorb the proteins for ELISA; 1.3 cm-by-1.3 cm in dimension.

(3) filter paper: to guide the liquid, reduce the impact of vacuumm and the deformation that might break the fiber mat.

(4) plastic plate: to guide the liquid and concentrate the flow in the central 3 mm diameter hole.

(5) rubber ring: to avoid leakage during the vacuum.

(6) sink/drain: to drain the liquid.

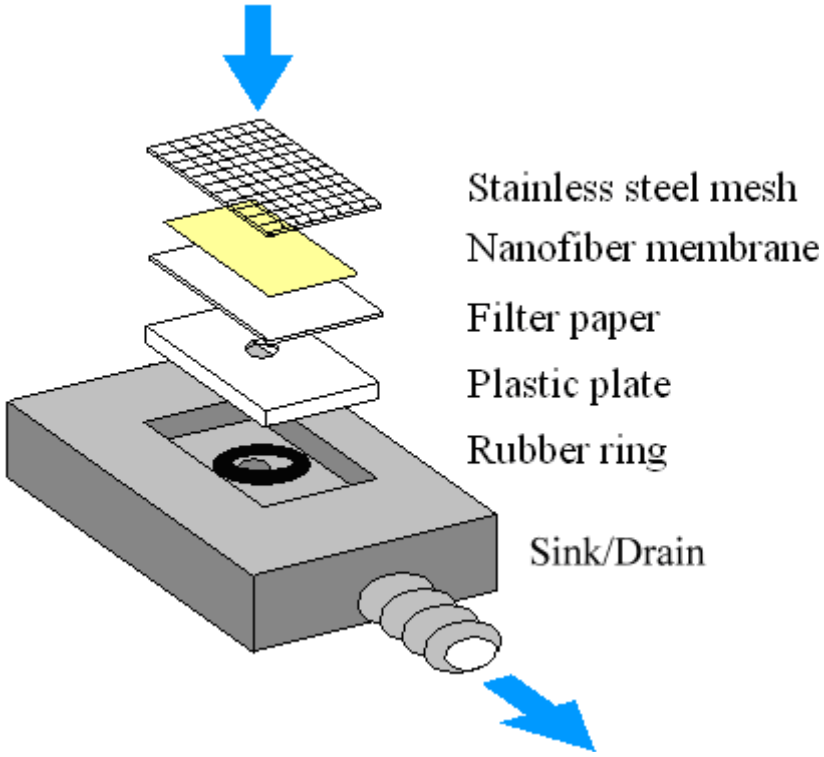

Figure 2. Layered structure of the nanofiber membrane device. Arrows indicate the direction of flow of the solution.

The device was evaluated based on the abovementioned methodology. Briefly speaking, the device should show differences between the sample with target molecules and the negative control. The target molecule was simulated by the matched secondary antibody (goat anti-mouse HRP) that can conjugate with the primary antibody. Typical procedures using this ELISA device involve dispensing reagents on the fiber mats and meanwhile removing them using an adjustable valve to control the drain speed, which are described as follows:

(1) Primary antibody coating: 3 ml of primary antibody (monoclonal mouse anti-c-Myc antibody, 5 μg/ml); slow drain.

(2) Wash: 2 ml of wash buffer solution (Tween 20/PBS); fast drain.

(3) Blocking: 3 ml of blocking agents (BSA, 4% in PBS); slowly drain.

(4) Wash: 2 ml of wash buffer solution; fast drain.

(5) Secondary antibody coating: 2 ml of secondary antibody (goat anti-mouse HRP or donkey anti-goat HRP, 3.1 and 12.5 ng/ml each); slow drain.

(6) Wash: 3 ml of wash buffer solution; fast drain.

The time was less than 3 minutes for fast drain and 10-15 minutes for slow drain. The purpose of slow drain was to increase the chance of protein adsorption or specific binding. The fiber mat was then removed from the device and immersed in substrates (Glo Substrate Reagent Pack, R&D Systems) for 5 seconds. The catalyzed substrates and those from traditional ELISA were measured together using an ELISA plate and compared.

2.2.3 Minimum Detection Limit

The minimum detection limit of the fiber mat was investigated following similar procedures as described in the Specific-binding experiments. Diluted enzyme-linked secondary antibody, ranging from 0 to 1.5 ng/ml, was used to catalyze the substrate. The more sensitive luminometer (TD 20/20, Turner Designs) instead of the ELISA reader was used to measure fluorescence strength.

2.3 Results and Discussion

2.3.1 Scanning Electron Microscope Characterization of Electrospun Silica Nanofibers

SEM images of silica nanofibers fabricated with different process parameters (Figure 3) show that the diameter of electrospun silica nanofibers was influenced by both the concentration of PVP and the volume ratio of SOG. It is found that the average fiber diameters generally decreased as solute concentration (the PVP concentration or SOG volume ratio in the solution) decreased or as the applied voltage increased (Figures 4). The polymer solution with SOG less than 80% of the volume ratio was found to result in fibers with diameters of less than 150 nm without much influence of applied voltage. The standard deviation of fiber diameter obtained at each voltage was found increased when the average diameter was larger. Thicker fibers were occasionally observed in the form of two merged fibers.

These SEM images were also used for estimating the porosity and the surface-to-volume ratio of the electrospun fiber mat. (Figure 5) The porosity, shown as pore ratio, was defined by dividing the area that was free from fibers by the total area of the SEM image. Porosity was found to decrease when deposition time increased, which was reasonable since the gradually accumulated fibers on the collector would result in thicker fiber mat and smaller pores in average. The surface-to-volume ratio was calculated by dividing the surface area of a fiber by its volume. For example, the electrospun fibers with 50 to 400 nm in diameter have the ratios ranging from 8×10^7 to 10^7. The porosity and the surface-to-volume ratio of the fiber mats that were used in the experiments were 0.0685 and 4×10^7.

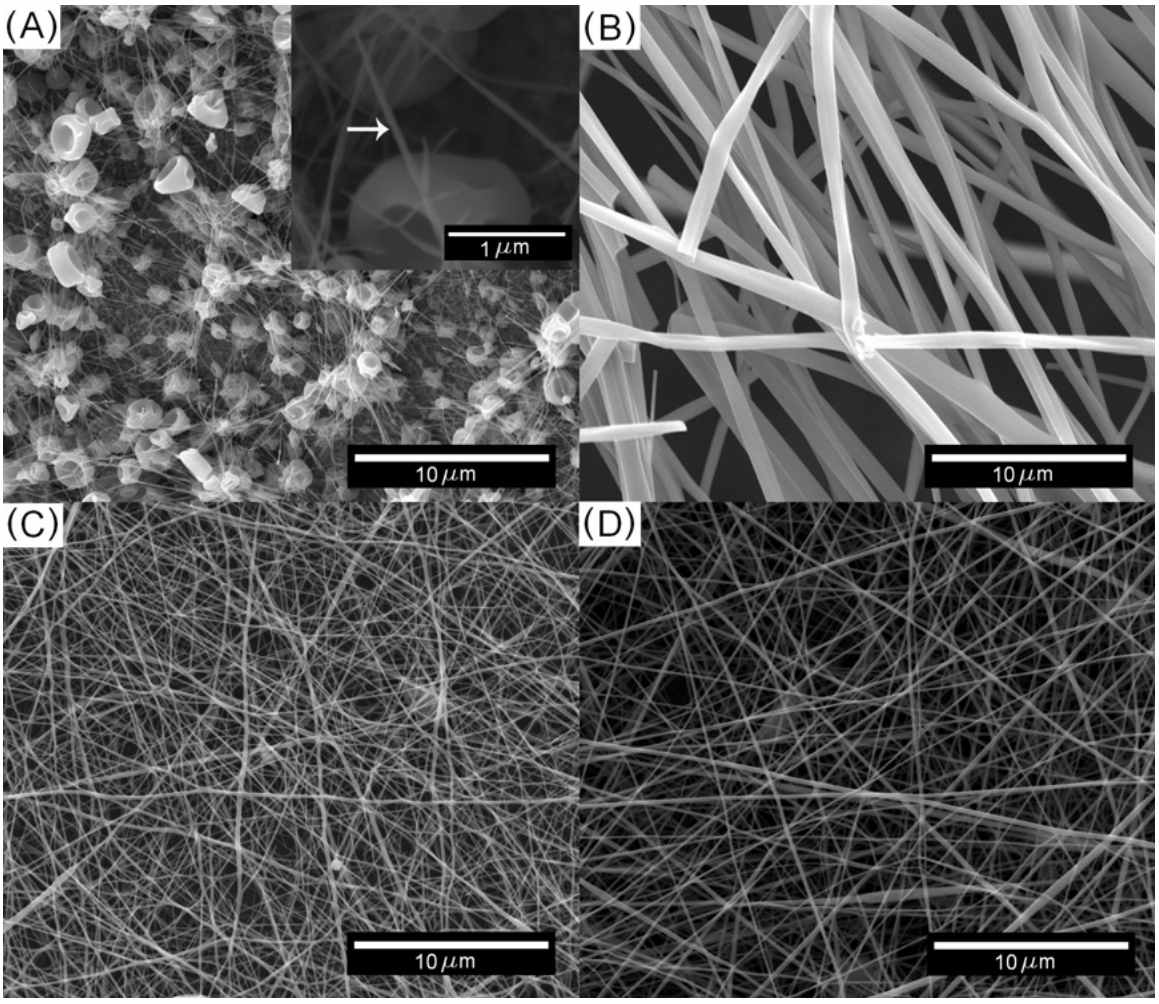

Figure 3. Scanning electron micrographs showing the diameters of electrospun silica nanofibers fabricated with various concentrations of PVP and volume ratios of SOG. (A) PVP, 0.02 g/ml; SOG, 100%, the inset shows a electrospun nanofiber with 57 nm in diameter. (B) PVP, 0.06 g/ml; SOG, 100%. (C) PVP, 0.04 g/ml; SOG, 40%. (D) PVP, 0.04 g/ml; SOG, 80%. The following parameters were kept constant for all experiments: feeding rate of 8 μl/min, deposition distance of 5 cm, applied voltage of 7 kV, needle size of 24 gauge, and calcination temperature of 773 K for more than 12 hours.

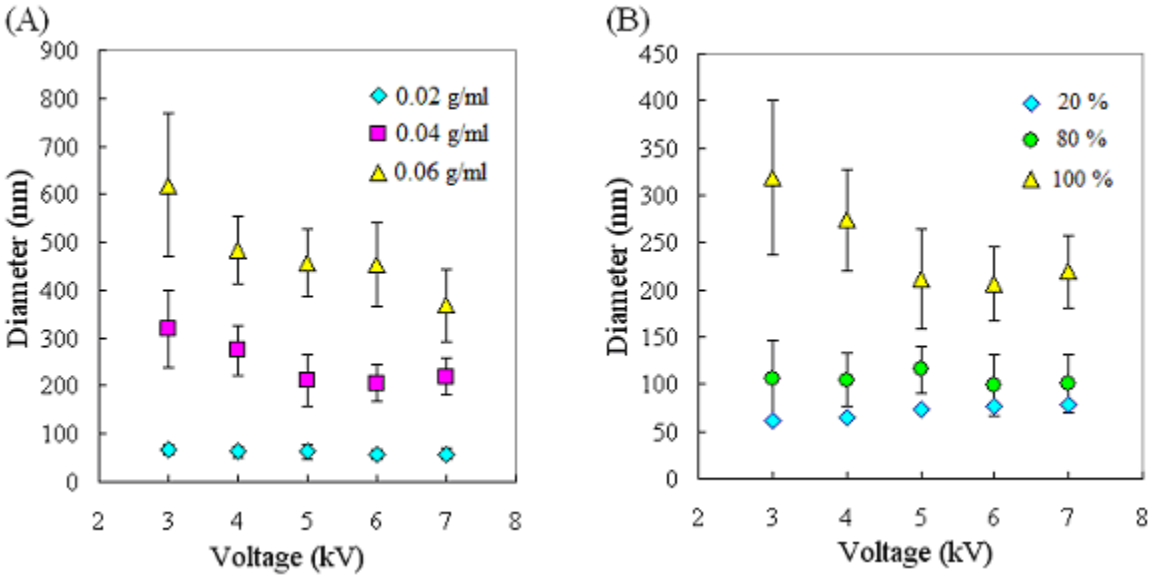

Figure 4. (A) The diameter of calcined silica nanofibers as a function of applied voltages for different PVP concentrations. (B) Nanofiber diameter as a function of applied voltages for different SOG concentrations.

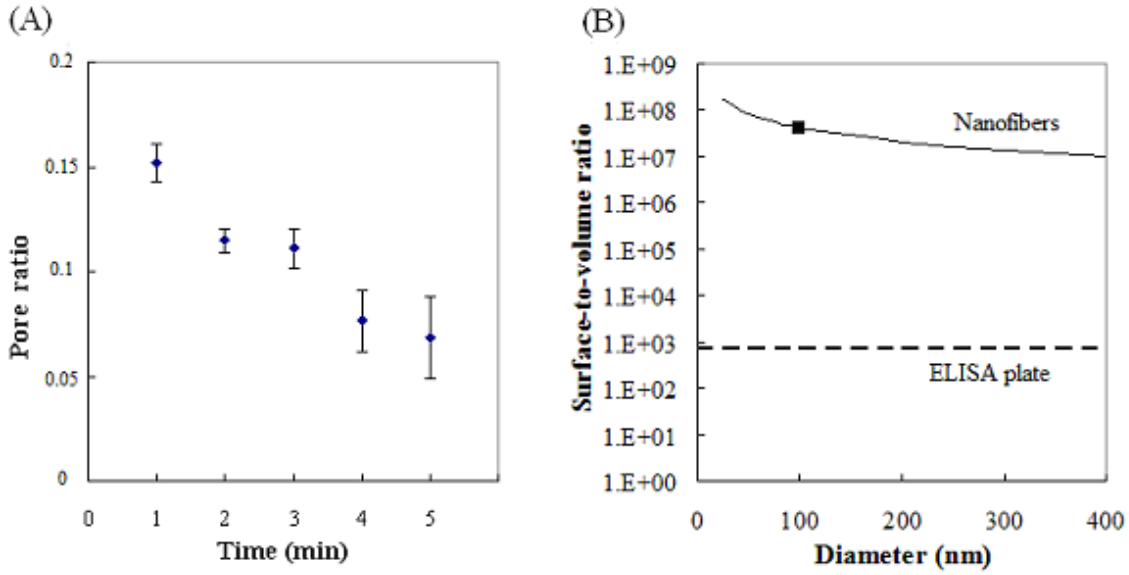

Figure 5. (A) Pore ratio as a function of deposition time. (B) Surfaceto-volume ratio as a function of the diameter of nanofibers and the ELISA plate. The square indicates the surface-to-volume ratio of the nanofiber membrane used for protein detection. The surface-to-volume ratio of the ELISA plate is defined as the inner surface area of a single well divided by its volume.

2.3.2 Nonspecific Binding of Protein on Electrospun Silica Fiber Mat

The x-ray films recorded the fluorescence (shown as dark areas on the films) from the slides for 10 seconds of short exposure and 2 minutes of long exposure, following the addition of substrate. (Figure 6) Long exposure time helped to locate weak fluorescence signals that were not detected in short time. The gray-scale images, converted from the scanned x-ray films, were used to estimate the differences. By defining pure white as 0% and pure black as 100%, the emission efficiency of each condition was calculated from its average gray-scale value within the square area. Under this definition, the emission of site A (negative control) and site B (primary antibody) were 11.3% and 20.8% for short exposure, and 14.1% and 56.5% for long exposure. A similar experiment was conducted on a plain glass slide, which showed much weaker adsrption. (Figure 7) These results confirmed that: (1) the high surface-to-volume ratio of electrospum silica fiber mat resulted in better protein-attachment ability than that of the plain glass slide, and (2) the procedures associated with specific binding of antibody and antigen in the ELISA technique can also be applied to the electrospun nanofiber membrane.

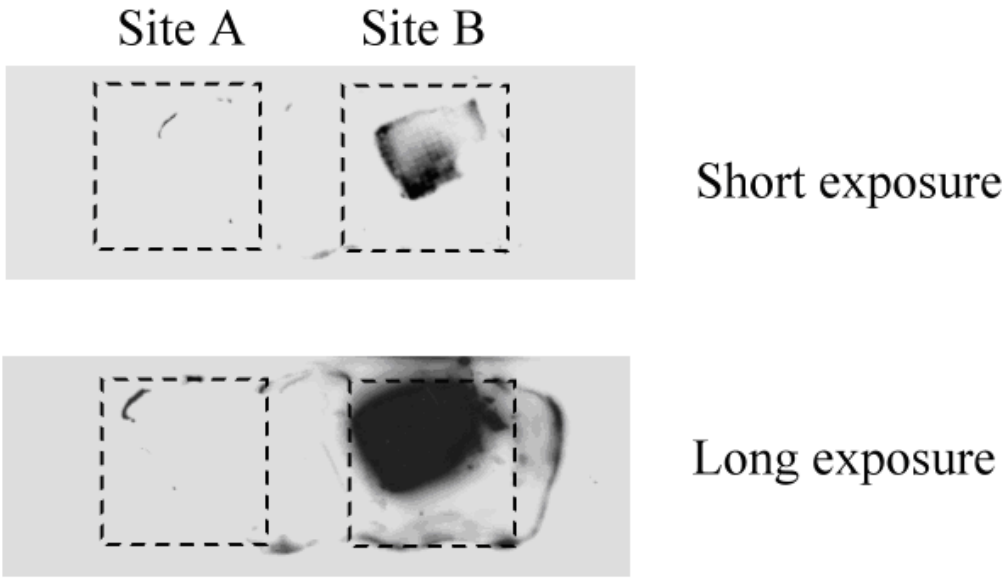

Figure 6. X-ray photos after 10 seconds short exposure and 2 minutes long exposure for the protein-attachment test on electrospun silica nanofiber membranes. Site A: results using BSA as negative control. Site B: results using primary antibody.

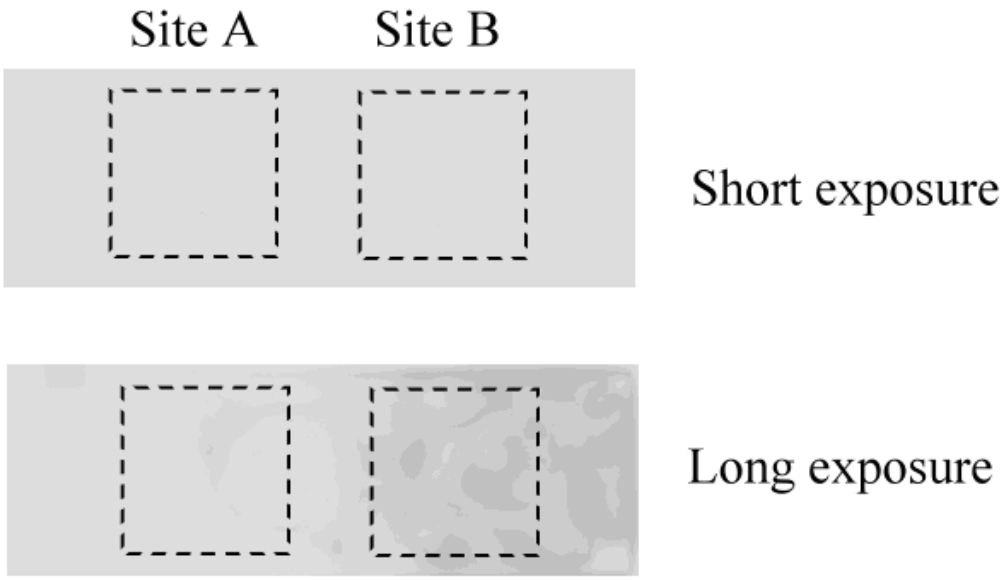

Figure 7. X-ray photos after 10 seconds short exposure and 2 minutes long exposure for the protein-attachment test on a plain glass slide. Site A: results using BSA as negative control. Site B: results using primary antibody.

2.3.3 Specific-Binding of Primary and Secondary Antibody

Results of the specific-binding experiments using the matched secondary antibody (anti-mouse) and the negative control (anti-goat) on platforms of the traditional one (ELISA) and the electrospun silica fiber mat (nanofiber) are shown in Figure 8. For each concentration of secondary antibody, we can easily discover that (1) the signal strength from the matched one using electrospun silica fiber mat was the highest, and (2) the differences of signal strength between the matched one and the negative control using electrospun silica fiber mat were more distinct than which using traditional ELISA. These results also suggested that the detection limit could be further lower using the electrospun silica fiber mat.

2.3.4 Minimum Detection Limit

The methodology we looked for the minimum detection limt was by finding minimum concentration of target molecules (secondary antibody) emitting signal strength barely distinguishable from the zero concentration (sample without any target molecules). Since the signal strength measured directly from the luminometer had the unit of relative light intensity (RLU), which was a relative value, the measured RLU values were all normalized by setting the value at zero concentration as 1. Average and standard deviation were calculated from 6 measurements of every concentration of target molecule. The results of previous section implied the limit might locate at concentration lower than 3.1 ng/ml, therefore we started our investigation from 1.5 ng/ml. The results show the minimum detection limit using the electrospun fiber mat was about 0.19 ng/ml

or 1.6 pM, and a good linearity in low concentration range. (Figure 9) When compared with the results from traditional ELISA, which had minimum detection limit at 6.25 ng/ml, electrospun silica fiber mat improved the detection limit for about 32 times. (Figure 10) These outcomes suggested that higher surface-to-volume ratio indeed improved the detection limit, and the target molecule of picomolar concentration may be estimated by performing linear interpolation on a known curve.

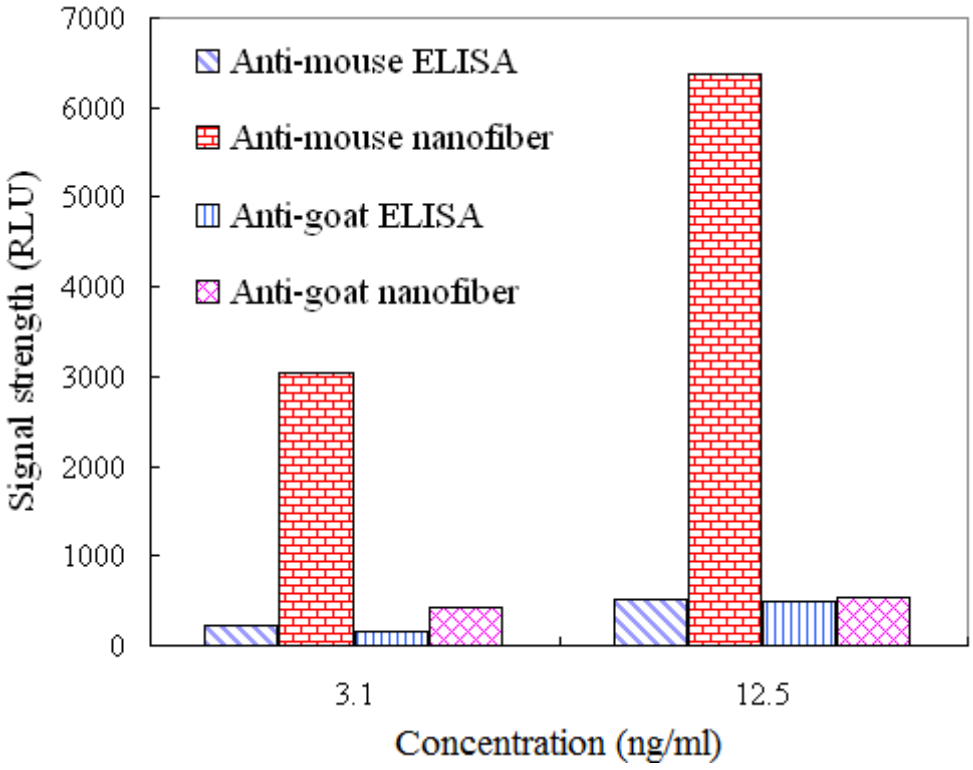

Figure 8. Signal strength (relative light unit, RLU) of specific and nonspecific-binding experiments performed using conventional ELISA and electrospun silica nanofiber membranes. From left to right for each experimental condition: specific binding on the ELISA plate, specific binding on the membranes, nonspecific binding on the ELISA plate, and nonspecific binding on the membranes. These results indicate that electrospun silica nanofiber membranes have much better sensitivity than does conventional ELISA.

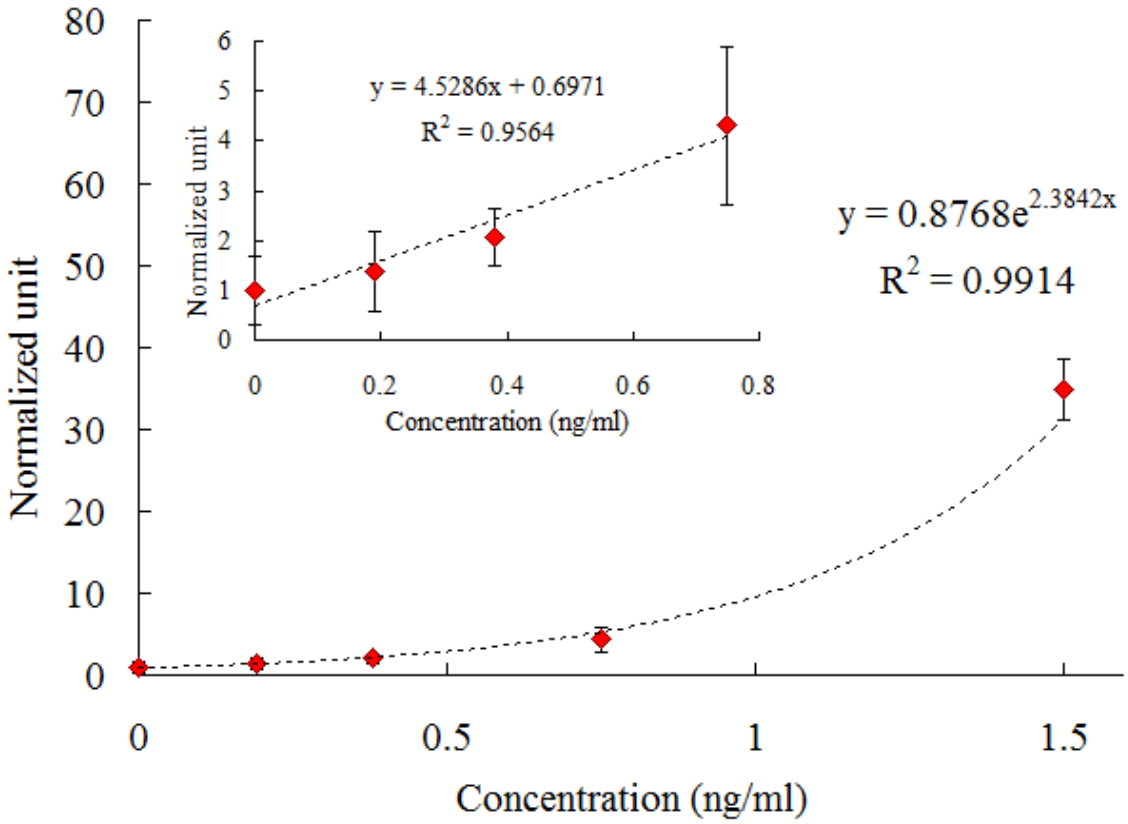

Figure 9. Normalized signal strength as a function of secondary antibody concentrations on electrospun silica nanofiber membranes. The inset graph illustrates the linear relationship at low concentrations. The average fiber diameter of the membranes is 100 nm with standard deviation 30 nm.

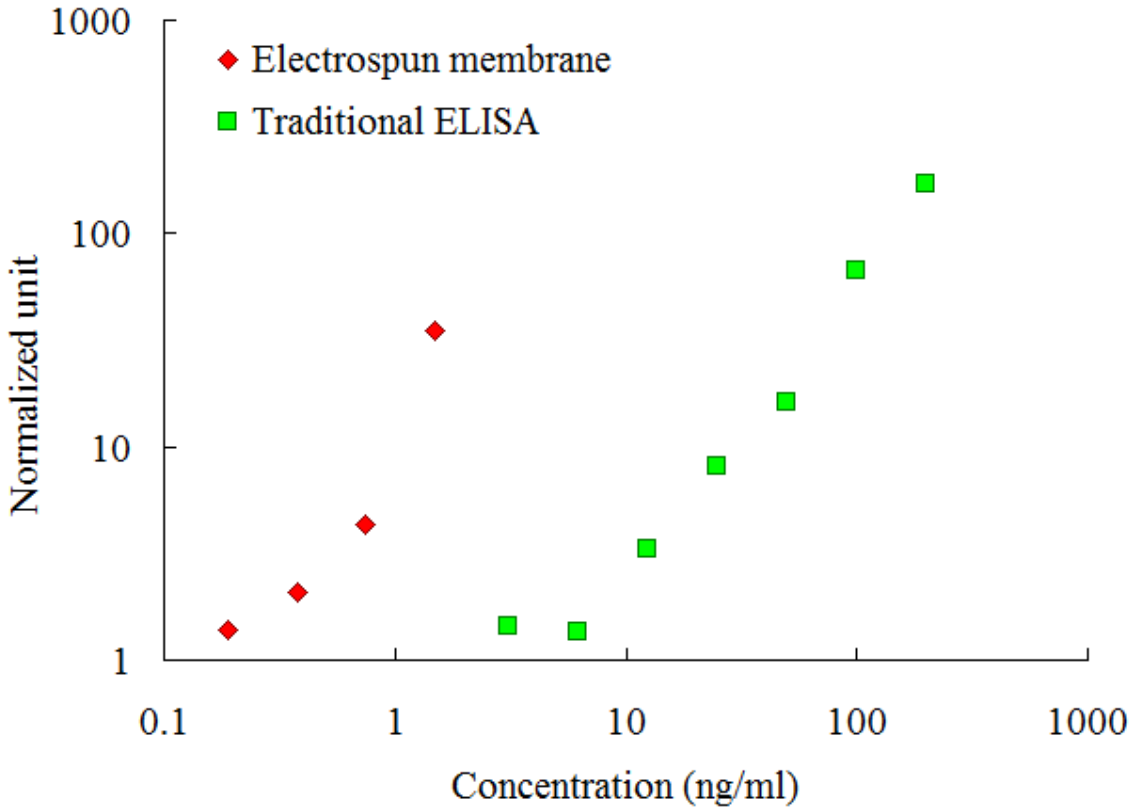

Figure 10. Detection results of electrospun nanofiber membrane biosensor and traditional ELISA.

In additional to the concern of detection limit, this membrane-based method has the advantages of short experimental time and reduced material costs. Traditional ELISA requires a long overnight incubation, because the diffusion-driven molecules have to travel much longer distance to attach the surface and to interact with other molecules. Each well of the plate has to be filled with a certain amount of reagents in each step, but only molecules near the well surface can participate in the reaction. On the other hand, the approach using electrospun silica fiber mat force most molecules in the volume of

reagents to travel trough the porous structure of the membrane by the external vacuum source. The molecules can therefore have much higher probability to contact the surface. The time for non-specific binding of protein or specific antibody-antigen interaction can be less than 15 minutes in each step. This improvement only requires 40 μl of solution for fabricating the 1.3 cm-by-1.3 cm electrospun fiber mat and the followed calcination.

2.4 Summary

A new electrospun silica membrane-base sensor device for biomolecules was studied. The dimension of the electrospun nanofiber was controlled by process parameters of electrospinning, such as electric field strength and polymer concentration. This biosensor drove the reagents by external vacuum source, forcing molecules to travel through the porous membrane. The much higher surface-to-volume ratio of the electrospun silica fiber mat resulted in better detection limit of target molecules than traditional ELISA. The linearity in low concentration range can be applied to detect target molecules down to picomolar concentrations. Compared to the 1 day of traditional assay, this new detection method only takes as short as 1 hour for all procedures of an experiment. The much shorter experimental time makes this electrospun silica membrane-base sensor device an ideal candidate for biomolecule and POC applications.

3. ANODIC ALUMINUM OXIDE MEMBRANE FILTER DEVICE FOR BACTERIA VIABILITY DETECTION

3.1 Introduction

The purpose of the project is to reduce the time in antibiotic efficacy tests by using anodic aluminum oxide membrane (AAO) membranes. The background knowledge of traditional methods monitoring bacteria viability against antibiotics, and the AAO membrane is introduced.

3.1.1 Bacteria Viability against Antibiotics

The growth of bacteria reflects whether the environment they stay is favorable or not. Bacteria continue to multiply until that the supportive resources are depleted or the multiplcation is interrupted by external factors. By observing the growth of bacteria against antibiotics, a clinician can select a proper antibiotic to treat bacterial diseases with less chances inducing antibiotic resistance. For example, patients receiving intubation in Intensive Care Units often catch ventilator-associated pneumonia (VAP) when the intubation is longer than 2 days. It is because pathogens, such as Staphylococcus aureus, Pseudomonas aeruginosa, and Enterobacter species, can directly infect the lung through the endotracheal tubes, resulting in 24 – 50% of mortality rate. Some studies showed that this high mortality for VAP patients may be attributed to inadequate antimicrobial treatment and increasing antibiotic resistance of pathogens, and may be resolved by rapid determination of initial antimicrobial drugs.[74-77] Currently,

several methods that can evaluate antibiotic efficacy are available, such as disc diffusion, Etest, broth dilution, or agar dilution methods. In these methods, the effect of antibiotic is quantified by minimum inhibitory concentration (MIC), which is the minimum antibiotic concentration that can prevent the growth of bacteria.[78-85] Researchers who want to know the MICs may observe the differences of bacterial growth under the effect of antibiotics after overnight incubation, whether in the form of bacterial colonies on an agar plate or the turbidity of a solution. For example, in disc diffusion or Etest methods, the bacteria suspension is first inoculated evenly on the surface of the agar plate with antibiotic discs or Etest strips placed on it. The MIC is measured by the diameter of bacteria-free zone on the next day. In agar or broth dilution methods, the bacteria suspension is inoculated on a series of agar plates incorporated with different concentration of antibiotic, or inoculated into tubes with broth solution and various concentration of antibiotic. The MIC is the minimum concentration that has no colony on the agar plate or has transparent solution after overnight incubation. The detection time for these tests to determine the efficacy of antibiotics is usually more than 24 hours. This delay may result in increase risk of hospital mortality, during which the antibiotic-resistant bacteria may worsen the infection.[86]

This 1-2 days duration is required because bacteria have to keep multiplying until visible differences form among the several antibiotic concentrations. The comparison requires the information such as the numbers of colonies in agar dilution method, the optical density number in broth dilution method, and the diameter of the bacteria-free zone in disc diffusion and Etest methods. Essentially, the methods presenting bacterial

viability affect the length of the experimental time. Therefore, the delay can be reduced if rapid monitoring of cell viability and better detection limit are achievable.

3.1.2 Anodic Aluminum Oxide (AAO) Nanoporous Membrane

In the membrane separation field, polymeric membranes are commonly used because of their low cost and wide availability on the market.[87] The choices of polymeric membranes are abundant, such as cellulose acetate, nitrocellulose, cellulose esters, polysulfone, polyether sulfone, polyacrilonitrile, polyamide, polyimide, polyethylene, polypropylene, polytetrafluoroethylene, polyvinylidene fluoride, polyvinylchloride.[88] The inorganic option made of aluminum oxide, AAO nanoporous membrane, actually had once been commercialized for years by Whatman Ltd.[89] Compared with any polymeric porous membrane, AAO membrane has features such as more uniform pore size, higher porous density, more parallel pore alignment, more rigid and flatter. These advantages of AAO membrane are the results of its complete different fabrication processes. The dimension of pore can be controlled precisely by using optimal fabrication parameters such as electrolyte, applied voltage, temperature, etc. in anodic oxidation process.[90] Most applications of AAO membranes have concentrated in the fabrication of nanostructures.[91-103]

So far, the applications of AAO membranes directly in biological field are limited and their potentials in antibiotic screening have not been fully explored.[104-106] As previously described, rapid monitoring of cell viability and better detection limit can result in faster evaluation of antibiotic efficacy. These criterions could be satisfied by

adapting a functional fluorescent stain SYTO 9 and the membrane filtration method. SYTO 9 green-fluorescent molecules can label cells by binding to their nucleic acids. The membrane filtration method can concentrate distributed cells at any moment of bacterial multiplication, and the features of the commercial AAO membrane making it ideal for such application. For that reason, a rapid antibiotic screening device consisted of an AAO nanoporous membrane and an incubation reservoir was made and applied to antibiotic efficacy test. Conceptually, bacteria in the sample and the antibiotic to be tested were reacted in the reservoir. Affected by the antibiotic, the bacterial multiplication was interrupted, resulted in ruptured cell walls. The bacteria were then filtered and stained on the AAO membrane. Ruptured bacteria were broken in pieces and drained during the filtration; live bacteria remained on the AAO membrane. The effectiveness of the antibiotic for the bacteria was determined by comparing the numbers of cells on the fluorescence image of the membrane over time.

3.2 Experimental

3.2.1 Detection Device and Equipment

A filter-device incorporating 0.22 μm pore size aluminum oxide membrane (Anodisc 13, Whatman) was used to trap E. coli and S. aureus which have the size of 1-2 μm. AAO membrane is inorganic and does not react with any reagent in the experiments. The alignment of pore has only one direction and the variation of pore size is very small. These features provide better quality control of the experimental results over most polymeric membranes, in which the pores are created by radiation or fabrics, and the

alignment and size of pore can have broader distribution. This AAO membrane was sandwiched sequentially by rubber O-rings to avoid leakage, and plastic plates to fix the shape. A reservoir was attached to one side of the plate mainly for incubation. The size of the reservoir was about 12.5 mm in inner diameter and 10 mm in height. The dimension of the filter-device was designed as same as that of a common glass slide (7.5 cm by 2.5 cm) so that it could be placed on the stages of most microscopes. (Figure 11)

The equipments aiding the detection consisted of a vacuum unit and a microscopy unit. The vacuum unit was used to hold the device and drain the solution in the reservoir of the device by a vacuum pump. The microscopy unit contained a blue (473 nm) light-emitting-diode (LED) for excitation, an optical filter set (35002v2, Chroma) for separating the emitted green fluorescence from the blue light, a movable stage, and a digital camera (DP20, Olympus) for recording the fluorescence images. (Figure 12)

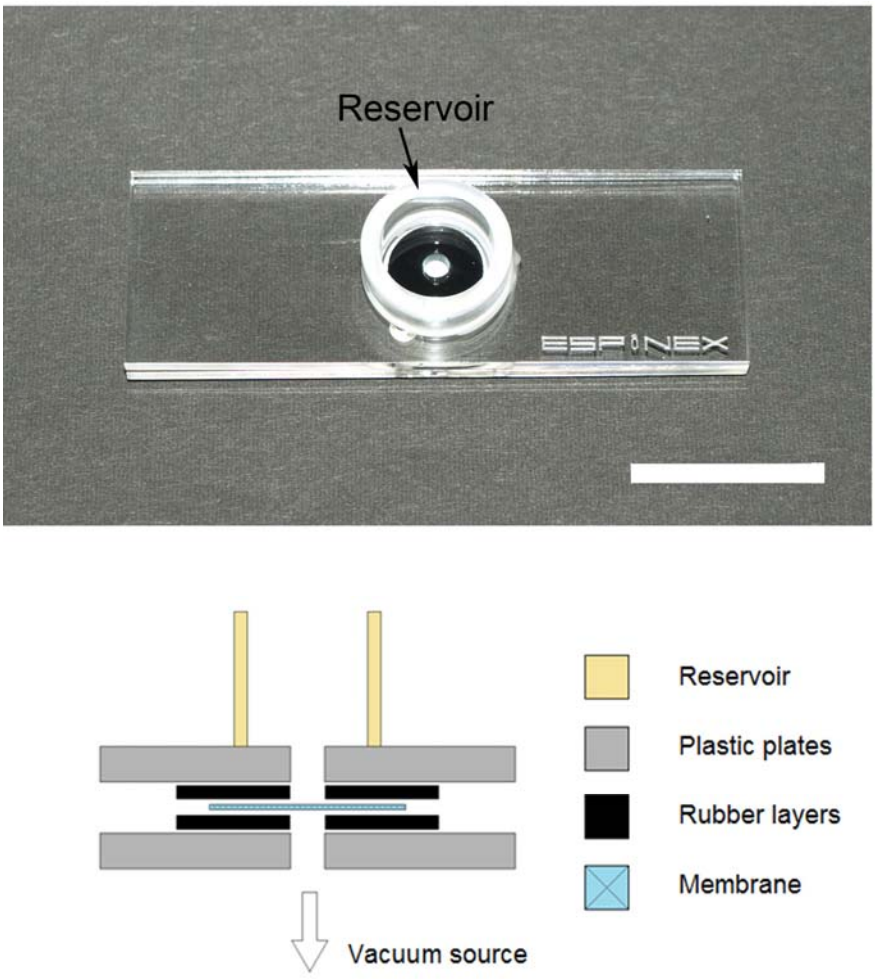

Figure 11. Photograph and schematic diagram of the assembled AAO membrane filter device for bacterial sensing. The scale bar is 2.5 cm.

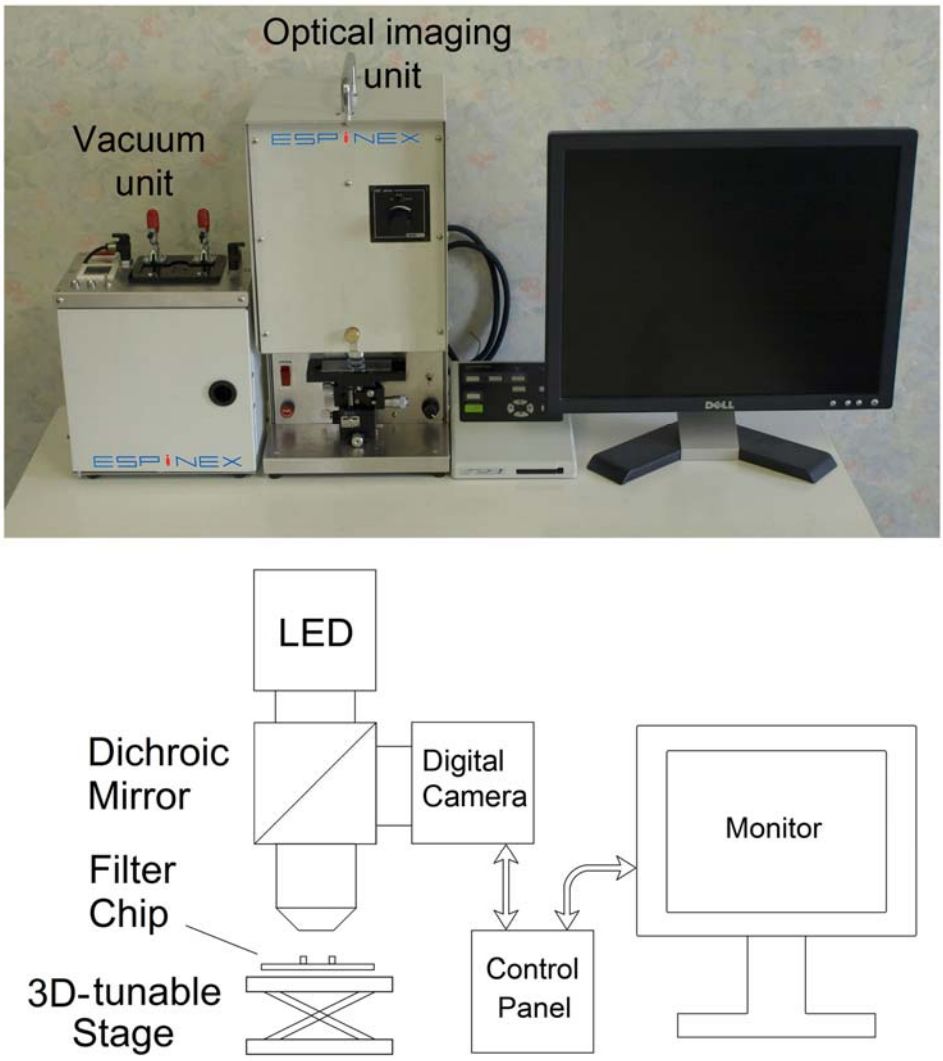

Figure 12. Photograph of the detection system. Top panel: the detection system includes a vacuum unit and a microscopy unit. Bottom panel: schematic diagram of the microscopy unit.

The green fluorescence stain used for staining the bacteria was prepared by dissolving SYTO 9 powder (Invitrogen) in 5 ml purified water. Typical fixation/staining of bacteria included following steps: a 100 µl sample solution was dispensed into the reservoir of a filter-device and drained. The cells on the membrane were then stained and washed. Staining procedures were performed after fixing the bacteria. The 50 µl stain solution was dispensed into the reservoir and drained immediately after 10 min of staining process. Excess stains were removed prior to the observation by flashing with 500 µl phosphate-buffered saline (PBS, AS ONE Corporation).

3.2.2 Calculation of Cell Number

The exact detection area was 0.76 mm by 1 mm for 10x objective lens. The size of each recorded image was 1200 pixel by 1600 pixel. The quality of each grayscale image was improved by ImageJ software to reduce background noise of the images. The cell number of bacteria on the membrane was determined based on following three steps. (1) A rectangular (600 pixel by 800 pixel) region of interest (ROI) that has the most bacterial cells was selected manually. The bright spots inside the ROI were viewed as cells, except the spots that were obviously too large. (2) Various single-cell regions on the same image were manually selected. These single-cell areas were compared to define a proper threshold value of grey-scale histogram and the average pixel size of single bacteria cell. (3) By applying the same threshold, total cell count in the ROI were calculated by dividing the signal area of ROI by the single-cell area. The quotient was

then times the ratio of the reservoir area over the ROI area. The product was viewed as the total cell count of the injected solution.

3.2.3 Calibration Curve of AAO Membrane in Bacteria Sensing

The methodology described in the previous section is actually an estimation of exact number of bacteria. The distribution of bacteria cells on the membrane and the selected ROI area may cause variations of the results. Therefore a calibration curve showing the relationship between the exact number of bacteria and the cell count using the membrane can provide a good reference of reliability.

E. coli K-12 bacteria in buffer solution (10^1 to 10^7 /ml) were used for calibrating the membrane. The staining procedures were the same as previously described. For comparison, the actual cell concentration of the same bacterial solution was also evaluated by counting colony-forming unit (CFU) on agar plates as in colony culturing method.

3.2.4 Monitoring Bacterial Growth with Antibiotic

To prove the concept that this membrane-base device could be used for antibiotic efficacy test, bacteria E. coli were incubated with antibiotic Pansporin and buffer solution PBS (negative control) respectively in the reservoir of the device, and observed at different time points. The mixture of 800 µl of liquid culture medium, 100 µl of Pansporin (1 mg/ml) or PBS for negative control, and 100 µl of E. coli solution (about 10^4 CFU/ml) was dispensed into the reservoir of the filter-device, followed by agitation

and incubation at 37°C using a shaking incubator (PIC-100S, AS ONE Corporation). Because the fluorescent stain might affect the bacterial multiplication, the devices at different time points were prepared separately. Three devices were prepared for 0, 30, and 60 minutes of incubations. After the incubation, the solution in the reservoir was drained using the vacuum unit. The staining, washing, and cell counting processes were the same as formerly described.

The influence of temperature was also studied by following the same procedures abovementioned but in room temperature instead of 37°C.

3.2.5 Determination of MIC

The susceptibility of bacteria to antimicrobial agents was determined by agar dilution method in accordance with the Clinical and Laboratory Standards Institute (CLSI) Guidelines. To determine the MIC, several concentrations of the antibiotic Pansporin (1 mg/ml to 10 ng/ml) and 100 μl E. coli solution (about 10^4 CFU/ml) were prepared for individual devices. These devices were incubated at 37°C in the shaking incubator and the number of survived E. coli was counted. The conventional agar dilution method, taking 24 hours for whole procedures, was used to confirm the results. In this test, the diluted antibiotic Pansporin solution was added into molten agar for the preparation of antibiotic-incorporated agar plates with various concentrations of the antibiotic. E. coli solution was then inoculated on each plate (1.5×10^4 CFU/plate). The MIC was determined after 24 hours of incubation.

3.2.6 Antibiotic Efficacy Testing for Patients' Samples

The device was used in the screening process of the antibiotics MPIPC and VCM on the MSSA and MRSA from patients' respiratory secretions provided by Saga Medical School Hospital, Japan. The sample type is sputum. The 800 μl liquid culture medium, 100 μl antibiotic solution (4 μg/ml for MPIPC and 20 μg/ml for VCM), and 100 μl sample solution (about 10^4 CFU/ml) were dispensed in series into the reservoir of a device without draining. The rest of procedures were as same as described in previous section for rapid antibiotic efficacy screening, except that the results were obtained right after 0, 60, 120, and 180 minutes.

3.3 Results and Discussion

3.3.1 Calibration Curve of AAO Membrane in Bacteria Sensing

The scatter plot of bacterial concentrations obtained by the conventional bacterial culture method as a function of the one obtained by the filter-device sensor system is shown (Figure 13). The R-square value of log-log fit was obtained as high as 0.9426, meaning that the AAO nanoporous membrane can determine the bacteria concentrations as precisely as the conventional bacterial culture method. Polycarbonate (PC) membranes, which are commonly used in bacteria sensing applications, were also tested under same conditions (not shown). However, the fluorescence outside the stained cells, caused by the absorption of the fluorescent stain on the surface of PC membranes, became considerably high noise. The pliability of PC membranes also impeded the focusing on the surface. In addition, the alignment of the pores in PC membranes is

randomly distributed, due to the track-etching process to generate pores. On the other hand, we found the rigidity, flatness, low background fluorescence, uniform pore size and parallel pore alignment in AAO nanoporous membrane made the AAO membrane a better candidate in this application.

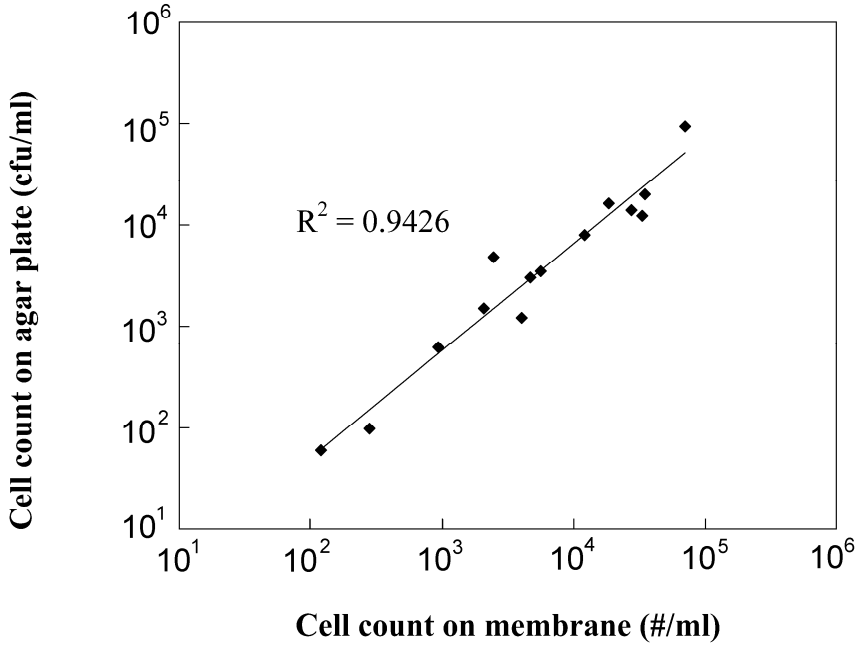

Figure 13. Scatter plot of cell counts from agar plate and filter-device. The high R^2 value suggests the device is reliable for bacterial enumeration at the range of 10^2 to 10^5/ml.

3.3.2 Monitoring Bacterial Growth with Antibiotic

Typical fluorescence images of the surface of membrane from the results of incubated solutions with and without Pansporin are shown in Figure 14. The number of bacteria in the sample solution with Pansporin was obviously less than that in the negative control sample immediately after 30 and 60 minutes. The SYTO 9 stained bacteria by binding to their nucleic acid. The green fluoresced objects were defined as live bacteria in our assay, since bacteria with damaged cell walls and membranes were easily ruptured and flushed away via pores when solutions were passed through the AAO membrane.

Number of bacterial cells remaining on the membrane was counted for each experiment. We defined the index of antibiotic efficacy (Index) to represent the changes of both sample and control with time:

$$\text{Index} = \text{Log}_{10}\{(N_x)/(N_0)\} - \text{Log}_{10}\{(C_x)/(C_0)\}$$

Where N_x and N_0 are the numbers of live cells from sample with the antibiotic at x and 0 minute, and C_x and C_0 are the numbers of live cells from negative control at x and 0 minute.

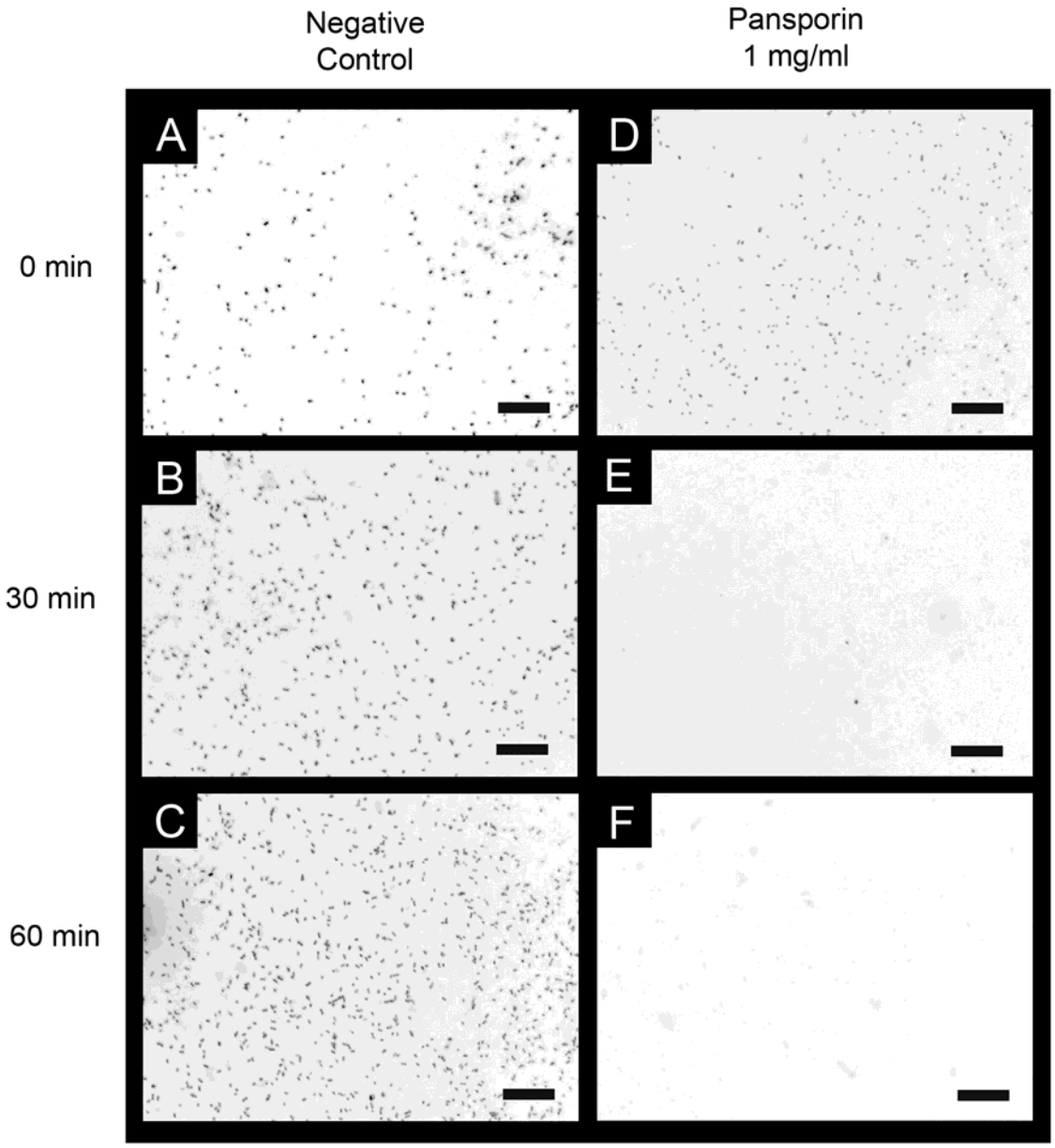

Figure 14. Color-inverted fluorescence images of E. coli (3.9 x 10^4 CFU/ml) on AAO membranes at different time of incubation process. Immediately after 0, 30, 60 minutes, the image of negative controls (A-C) and samples with antibiotic Pansporin 1 mg/ml (D-F). The number of bacteria with antibiotics obviously decreased, since the antibiotics had interrupted the bacterial growth. The scale bar is 50 μm.

In general, the number of bacteria increased with time in the negative controls ($C_x/C_0>1$), but decreased with time in the sample with the antibiotic ($N_x/N_0<1$). If an antibiotic has better efficacy for the tested bacteria, the index will have a more negative and steeper slope in our custom-defined index. The index was also applied to both cases with and without incubation.

Without incubation process, the enumeration showed live cell count was unstable in Pansporin after 60 minutes, either 45% increase or 33% decrease. On the other hand, the result with incubation showed homogeneous reduction (>98%) in live cell count after 60 minutes. Figure 15 shows a comparison of the antibiotic efficacies with and without incubation processes. It was obvious that the incubation is a required step to determine the antibiotic efficacy. This difference can be attributed to that most antibiotics, including Pansporin, are designed to disrupt the synthesis of bacterial cell wall during cell fission process. Since the optimal cell division of E. coli was at 37 °C, these results fitted our expectation and the index reasonably reflected the antibiotic efficacy on the bacteria.

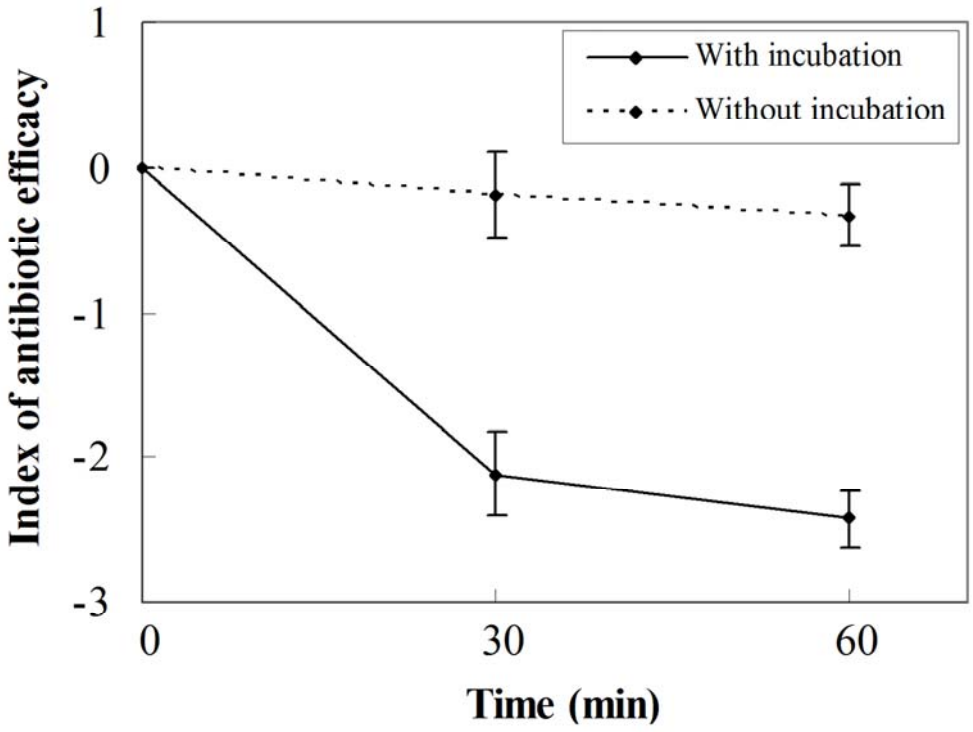

Figure 15. Index of antibiotic efficacy of E. coli as a function of time. The solid line has a steeper slope than the dotted line, meaning that the antibiotic requires incubation to take effect.

3.3.3 Determination of MIC

Figure 16 shows the fluorescence images of E. coli exposed to various concentrations of Pansporin with 0, 30, and 60 minutes of incubations. The reduction of the number of bacteria was obvious along observation time in the 1 mg/ml and even the diluted 1 μg/ml of the antibiotic concentration. However, there was no significant difference between the sample with 10 ng/ml Pansporin and the negative control.

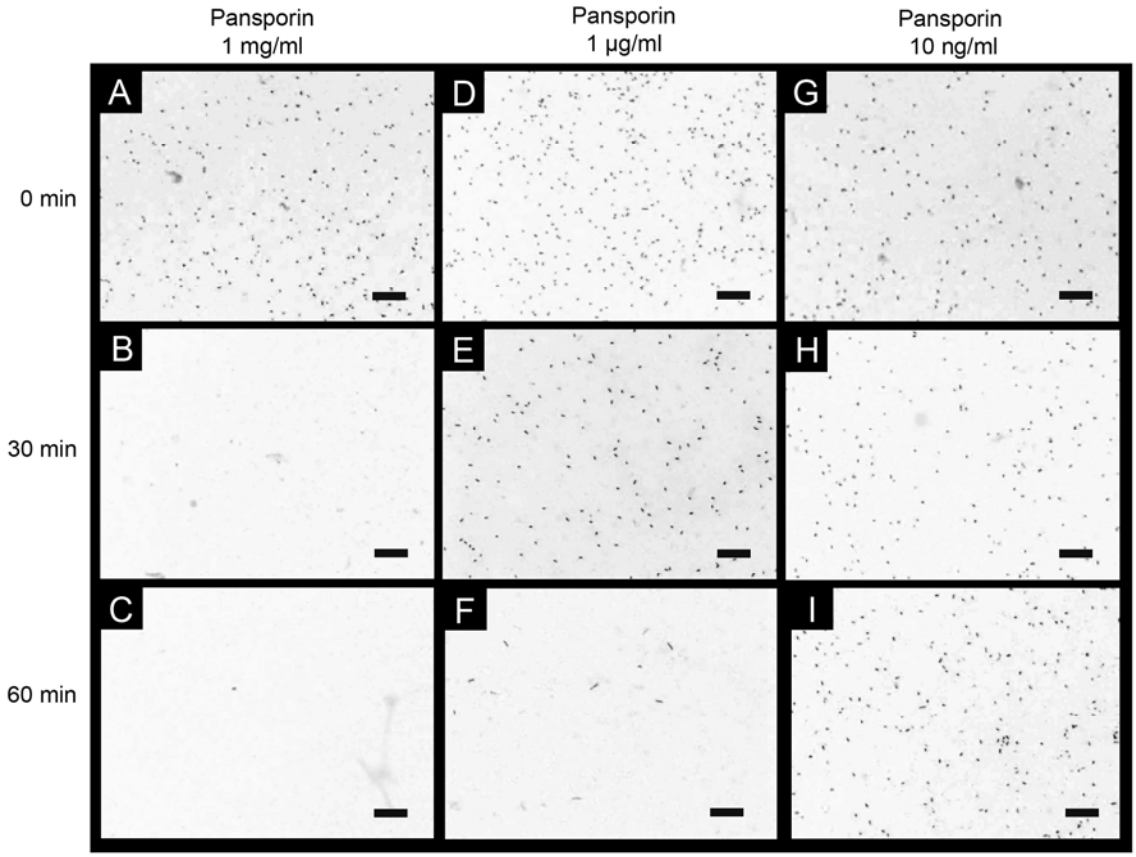

Figure 16. Color-inverted fluorescence images of E. coli on AAO membranes at different time and specific concentrations of the antibiotic with incubation process. Immediately after 0, 30, 60 minutes, the images of samples with antibiotic Pansporin 1 mg/ml (A-C), 1 µg/ml (D-F), and 10 ng/ml (G-I). The scale bar is 50 µm in width.

The graph of antibiotic efficacy index as a function of time indicates diluted antibiotics have fewer efficacies (Figure 17A). The slope was negatively proportional to the concentration during the 60-minute period for 1 µg/ml to 1 mg/ml. The slope was nearly horizontal for the 100 ng/ml sample for more than 1 hour, and the difference between 100 ng/ml and 1 µg/ml samples was noticeable. Accordingly, we estimated that the MIC of Pansporin was between 100 ng/ml and 1 µg/ml. This estimation was

confirmed by the conventional agar dilution method (Figure 17B). Our approach appears exceeding, as it took only 1 hour to determine the antibiotic efficacy compared to the typical 24 hours required for conventional techniques.

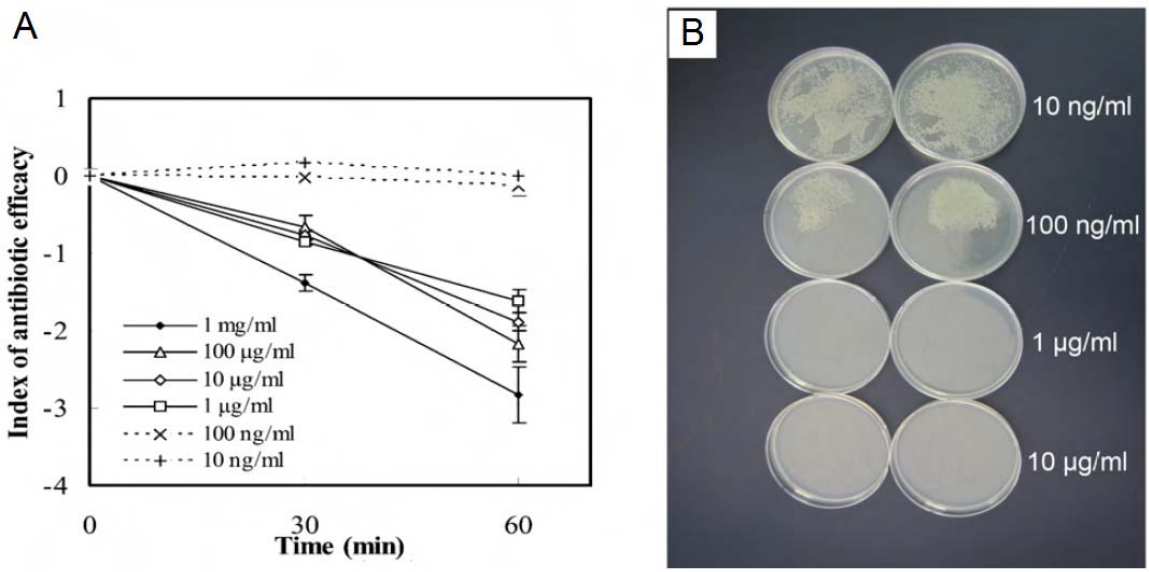

Figure 17. (A) Index of antibiotic efficacy as a function of time and Pansporin concentration. The antibiotic effect on the bacteria can be divided into 3 groups: ineffective for 10 and 100 ng/ml; effective for 1, 10, and 100 µg/ml; the most effective for 1 mg/ml. (B) Growth of bacteria using conventional agar dilution method. MIC is between 1 µg/ml and 100 ng/ml, which is the same as our estimation based on the filter-device system.

3.3.4 Antibiotic Efficacy Testing for Patients' Samples

This technique was furthermore applied to the screening of antibiotics for MSSA and MRSA samples from the patients in Saga Medical School Hospital. The fluorescence images of the results are shown in Figure 18, after their background noises

were subtracted using ImageJ. The cell growth of MSSA was reduced by the antibiotic MPIPC. For MRSA sample, the growth of MRSA was undeterred by MPIPC but interrupted by VCM. The index of antibiotic efficacy as a function of time is shown in Figure 19. In this graphs, the slopes of MSSA-MPIPC and MRSA-VCM samples were more negative with time than those of MRSA-MPIPC. The effectiveness of the two antibiotics was easily distinguishable in 1 hour.

3.4 Summary

We have developed a rapid antibiotic efficacy screening system by using a filter-device incorporating aluminum oxide nanoporous membrane. The MIC obtained by the filter-device system matched well with the one obtained by the conventional approach. Compared to the conventional antibiotic efficacy test using agar plate, the filter-device system can dramatically reduce the test time from 24 hours to 1 hour, aiding fast decision making of antibiotics in medical treatments. This test-in-vitro setup can help tailor antibiotic therapy, and reduce microbial antibiotic resistance by shortening antibiotic exposure on human body. Meanwhile, very small amount of sample is required for the test, and the procedures are feasible. Its simple design facilitates mass production of the filter-device as well. These characteristics make the filter-device system a potentially valuable tool in POC applications in the near future.

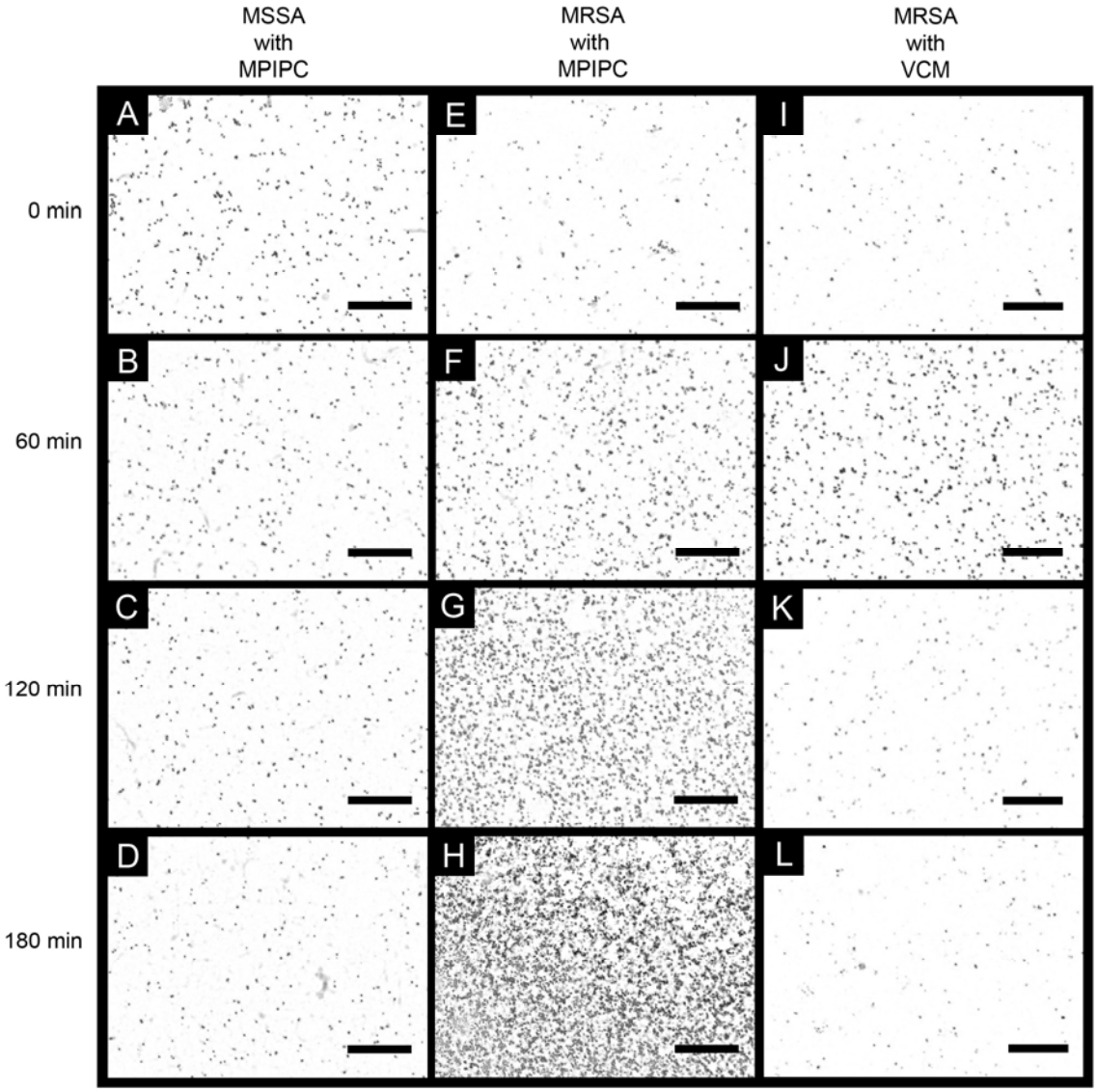

Figure 18. Color-inverted fluorescence images of MSSA and MRSA on AAO membranes at different time with incubation and antibiotics. Immediately after 0, 60, 120, 180 minutes, the images of MSSA samples with MPIPC 4 μg/ml (A-D), MRSA samples with MPIPC 4 μg/ml (E-H), and MRSA samples with VCM 20 μg/ml (I-L). The growth of MRSA was not affected by MPIPC, but impeded by VCM. The scale bar is 50 μm.

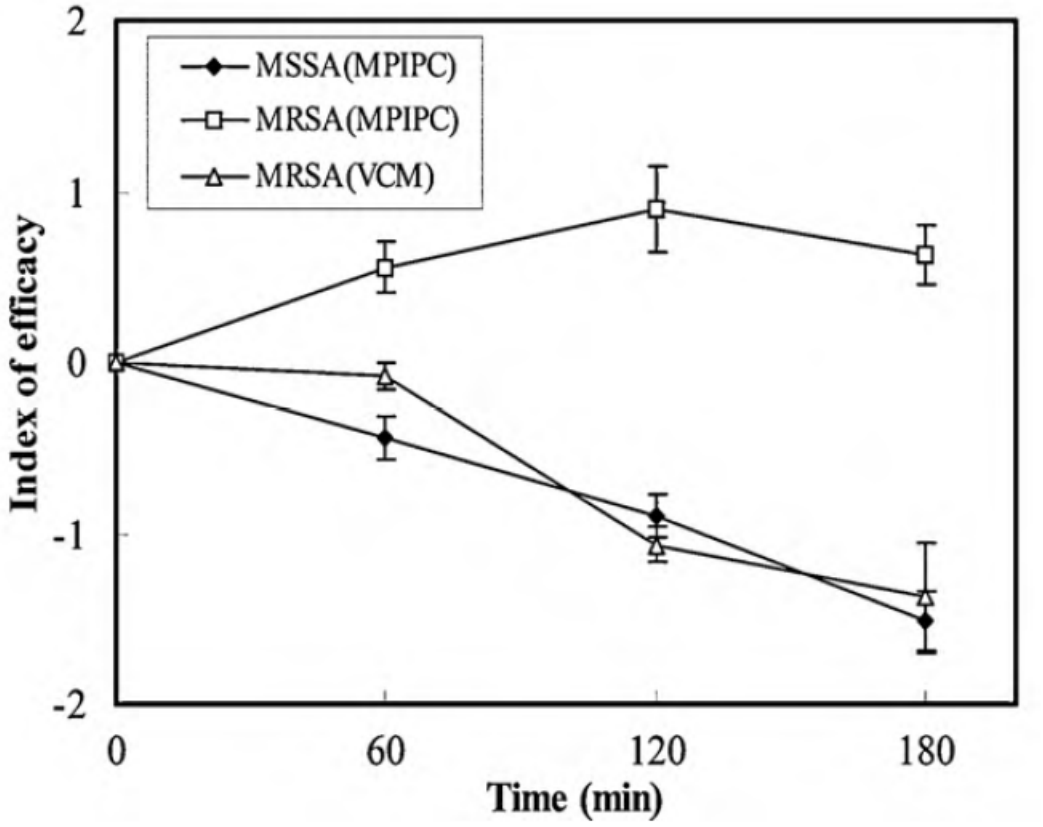

Figure 19. Index of antibiotic efficacy as a function of time and concentration of antibiotic MPIPC and VCM. The growths of MSSA and MRSA are reduced by MPIPC and VCM respectively.

4. MICROFLUIDIC/ELECTROSPUN MEMBRANE OPTOFLUIDIC DEVICE FOR SURFACE ENHANCED RAMAN SPECTROSCOPY

4.1 Introduction: Surface Enhanced Raman Spectroscopy

Raman spectroscopy is a spectroscopy used to study Raman scattering, and named after the Indian physicist C. V. Raman, who was devoted to the research of light scattering that led to the discovery of the scattering in 1928. Raman scattering is one of the several cases of the interaction between an electromagnetic (EM) wave and a matter, if we describe light as EM wave. When an incident monochromatic EM wave travels trough a material, it may induce oscillation of the electron clouds of the molecules or atoms. The oscillation of electrons becomes a source of EM wave and radiates with a new wavelength and direction. This phenomenon is the scattering of EM wave. Most of the induced EM waves have the same wavelength as the incident EM wave, which is defined as elastic scattering. A small fraction of the induced EM waves may have different wavelength from the incident one, which is defined as inelastic scattering. Raman scattering is one of the inelastic scattering cases, and the shift of the wavelength is caused by the interaction of the incident EM wave and the material, originated from the change of vibration and rotation energy states of molecules. The fraction of the inelastic scattering of EM wave is typically very small ($1{:}10^7$) and the intensity of Raman scattering is much weaker than the elastic scattering ones, so Raman scattering is not as noticeable as elastic scattering in most cases. The detection of Raman scattering usually requires a strong incident monochromatic source to induce, a good dichroic filter

to separate the scattered light from the incident one, and a sensitive receiver to sense the signals. The degrees of shifting between incident and scattered wavelength depend on the scattering material, and are usually expressed as Raman shift ($\lambda_{incident}^{-1} - \lambda_{emitted}^{-1}$) in the unit of ($cm^{-1}$). Raman spectrum of a molecule, shown as intensity versus Raman shift, is viewed as its fingerprint since it provides information down to molecular structures.

SERS is a surface-enhanced detection of Raman scattering, in which the Raman signals of the molecules are greatly enhanced by the rough metal surfaces absorbing the molecules. This improvement was accidentally found by Martin Fleischman and his coworkers in 1974 from pyridine adsorbed on electrochemically roughened silver.[107] Several different kinds of structures have also been explored, such as gratings,[108-109] island films,[110-112] colloids,[113-116] nanoparticle array,[117-122] nanorod arrays,[123-126] metal-coated nanoparticles,[127-128] and nanoshells.[129-135] The excitation of localized surface plasmon resonances on those structures contributes the amplification of light and result in the enhancement.[136] The "hotspots" describe the regions on the SERS substrate where the electromagnetic enhancements are the highest, and result in strong SERS signals of molecules. The signal enhancement, represented as enhancement factor, can be as large as 10^{14} at those hotspots.[137] However, locating the hotspots sites is prerequisite before acquiring SERS signals, and the adsorption of molecules on the surface of nanoparticles mostly rely on diffusion, which is random and has low reproducibility of experiments. Fabricating nanostructures using cleanroom instruments and techniques may improve the uncertainty of the hotspot position. Periodic metal nanostructures for a SERS substrate can be determined by photolithography prior to experiments. For example, the e-beam

lithography can fabricate metal nanoparticle array with designated shape and size,[117-121] or create template of wells for nanoparticle cluster arrays.[122] On the other hand, fabrication of these SERS substrates requires more complicate processes, which are often expensive. Long analysis time remains unsolved since analyte molecules still have to diffuse to the hotspots.

To address the aforementioned limitations, a novel optofluidic device integrating an electrospun silica nanofiber membrane and microfluidic channels was developed, which could provide significant sensitivity of SERS signal while drastically reduce fabrication cost. This optofluidic device has a unique junction with an electrospun silica nanofiber membrane sandwiched between the inlet and outlet channels, where gold nanoparticles adsorbing analyte can be trapped. The porous structures of the junction are smaller than the 60 nm gold particles, and the gold particles are aggregated at the junction along with target molecules when vacuum force is applied.

4.2 Experimental

4.2.1 Fabrication of Silica Nanofiber Integrated Optofluidic Device

The silica nanofiber integrated optofluidic device was fabricated by two independent processes: electrospinning and soft-lithography of polydimethylsiloxane (PDMS). Electrospinning was for depositing silica nanofibers on the glass slide, the bottom layer of the device; soft-lithography of PDMS was for preparing the microfluidic channels, the top layer of the device.

The polymer solution for electrospinning was prepared by mixing 6.4 ml of SOG solution (IC1-200, Futurrex, Inc.), 1.6 ml butanol (Solvent Diluent SD4, Futurrex, Inc.) and 0.32 g PVP (MW=1 300 000, Aldrich). The resultant mixture was an 8 ml of 80% SOG and 0.04 g/ml PVP solution. The polymeric composite solution was electrospun using 8 cm of deposition distance, 5 kV of voltage (Series 230, Bertan), 4 μL/min of pump rate (Pump 11 Plus, Harvard Apparatus), and a 24 gauge of stainless steel needle (Hamilton Company). The deposition area was confined by a custom-made plastic mask with a 3 mm-by-3 mm opening. The electric field between the needle and the large metal collector behind the glass slide allowed the deposition of nanofibers, which stayed firmly attached to the glass slide surface after the separation of the plastic mask and the glass slide. The deposited composite nanofibers were then calcined at 500 °C for 12 hours to remove the PVP and create pure silica nanofibers. Figure 20 illustrates fabrication of electrospun nanofiber membrane, and the scanning electron microscope (SEM) image shows the resultant electrospun membrane on the glass slide.

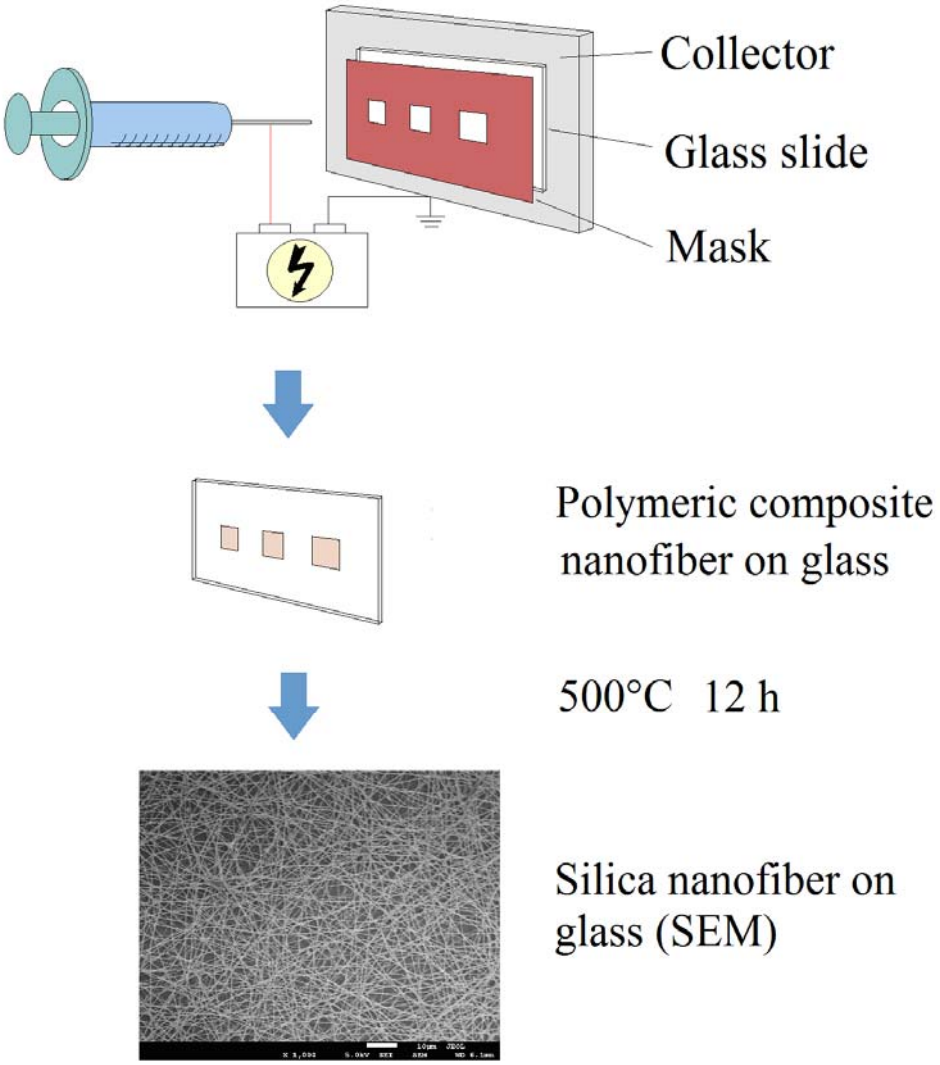

Figure 20. Fabrication process of the bottom layer of the silica nanofiber membrane integrated microfluidic device. The silica nanofiber membrane was deposited on a glass slide by electrospinning polymeric composite nanofibers, followed by the removal of the polymer at high temperature.

The PDMS microfluidic layer was fabricated by the conventional soft-lithography molding methods.[138-139] The mask for photolithography was designed using AutoCAD (Autodesk) and printed by CAD/Art Services Inc. The mold was made by

spin-coating (WS-650S, Laurell) photoresist SU-8 2025 (MicroChem Corp.) at 3000 rpm yielding a 20 μm thickness using 100 seconds of UV exposure (Q4000MA, Quintel) followed by developing and a hard bake. The PMDS layer was made by mixing base and curing agent (Sylgard 184, Dow Corning) at a 1 to 10 ratio, followed by a molding process at 70˚C for 2 hours. The chip was assembled using oxygen reactive-ion-etching treatment (CS-1701, March Plasma Systems) to bond the PDMS layer and the glass slide together as shown in Figure 21.

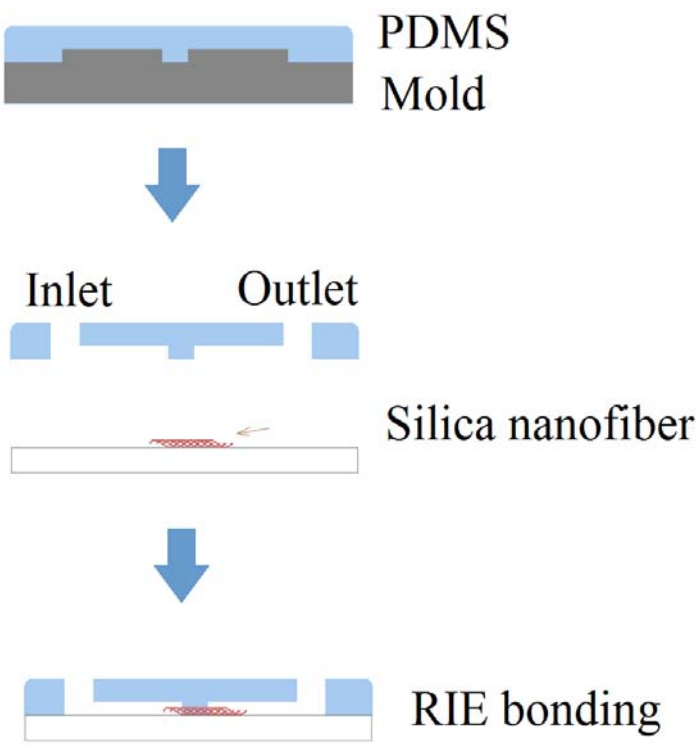

Figure 21. Fabrication and assembly process of the silica nanofiber membrane integrated microfluidic device. The PDMS microfluidic channels were fabricated via an SU-8 mold and bonded with the silica nanofiber membrane bottom layer.

4.2.2 Design of Channel Pattern

This optofluidic device was designed based on several known phenomena: (1) the flow of liquid favors the lowest resistive path; (2) surface variations of an electrospun silica nanofiber membrane on glass create nanopores; (3) these nanopores allow liquid to flow but block larger particles such as the 60 nm gold and analyte of interest. The distance of the junction between the front and rear section of the microfluidic channels was 25 μm, the shortest path for liquid to flow. (Figure 22) For such reason, the solution is expected to travel through this 25 μm channel junction, as shown by the red arrows in Figure 22, mechanically trapping the particles at the nanofiber membrane and encouraging the gold nanoparticles to accumulate at the channel boundary.

4.2.3 Trapping and Aggregation Test

In this study, the flow was driven by pressure difference between the inlet and outlet channels. Although both applying positive pressure at the inlet or negative pressure at the outlet should work, the latter one was adapted. The main consideration was to avoid the expansion of the volume inside the PDMS channel that might decrease the trapping ability if positive pressure was applied. Therefore, the outlet was connected to a 30 ml syringe, serving as a negative pressure source, to drive the liquid into the channel and pass through the 25 μm junction. The initial value of the negative pressure was estimated to be 1/60 atm (1.7 kPa) after considering the volume of tubing when the syringe was fully extracted.

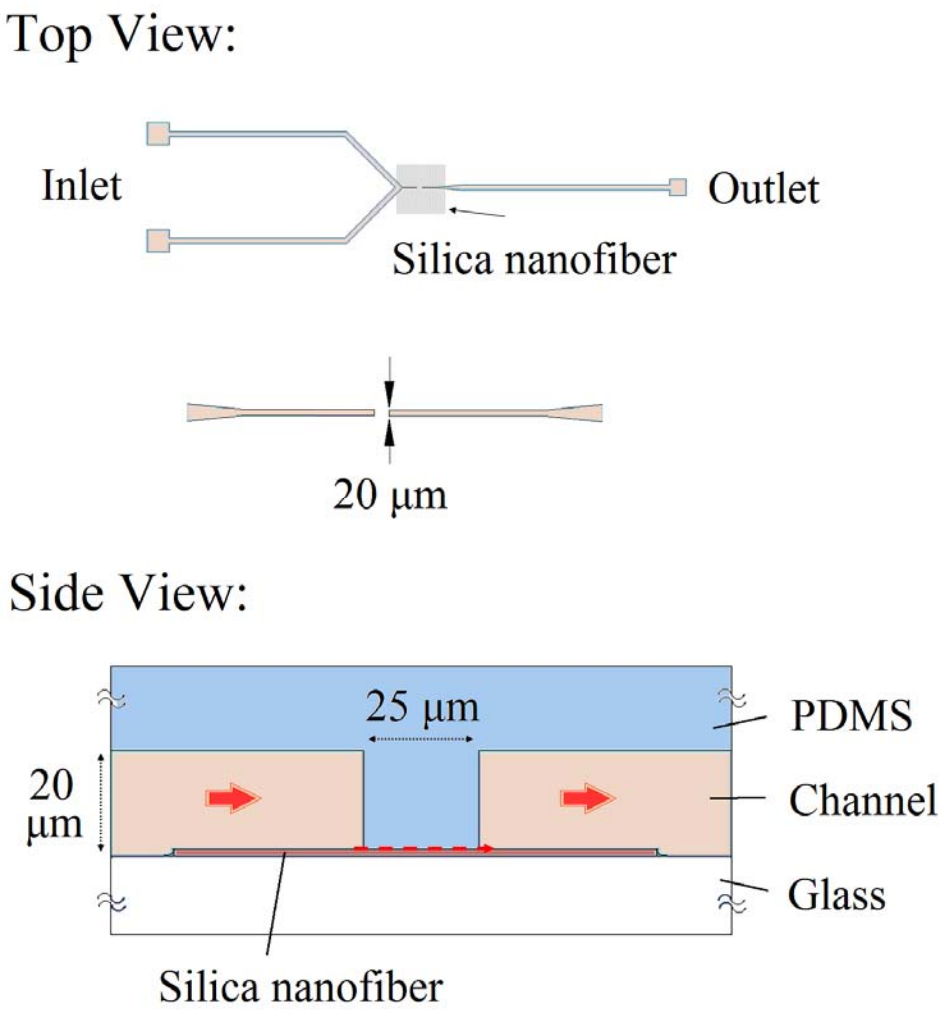

Figure 22. Schematic of the assembled device. Top view: the front and rear section of the microfluidic channels are bridged by the deposited silica nanofiber membrane; the lower panel is the enlarged view of the ends of the two channels. Side view: Red arrows indicate the flow direction. The nanopores created by the deposited nanofiber membrane enabled the flow through the 25 μm bridged region.

Particle trapping efficiency was evaluated by dispensing 20 μl of polystyrene (PS) beads, prepared from 1000 times diluted 1 μm PS microparticles (Sigma-Aldrich), into one of the inlet channels, followed by syringe-vacuuming with 1/3 of full extraction. The full extraction was not applied, because low pressure drop and the slower flow rate facilitated the observation of the aggregation process. Once the aggregation process had been shown with the PS microparticles, a similar experiment was conducted using 20 μl of 60 nm gold nanoparticles (Unconjugated PolyGold, Polysciences, Inc.) and syringe-vacuuming system with full extraction. Images were taken during the process of aggregation using a CCD camera (QuickCam Pro 4000, Logitech).

4.2.4 SERS Signal of Adenine

A solution of adenine, a known Raman active analyte, was used to investigate the performance of the silica nanofiber integrated optofluidic device as a SERS substrate. The maximum solubility of adenine in water was known as 0.976 mg/ml or 7.2 mM.[140] Four adenine dilutions of 100 μM, 10 μM, and 1 μM, and 0.1 μM in water were prepared from this saturated solution. Each concentration of adenine was then mixed with the 60 nm gold nanoparticles with a volume ratio of 1:10 (adenine:gold =1:10). SERS signals of the adenine solution were measured after dispensing 10 μl of adenine/gold solution into the device and vacuuming until the volume at the inlet channel appeared nearly empty. The signal was collected at the aggregation spots at the boundary of channel and nanofiber membrane. For the non-SERS Raman signal, due to

the insolubility of adenine in water at high concentrations, 1 M of adenine was dissolved in 1 M HCl, and this was used as the baseline to calculate the enhancement factor.

The Raman spectra for the concentration studies was measured using a Horiba Jobin-Yvon LabRam IR system, with 785 nm/8 mW laser source, 50 μm pinhole, 5 sec integration time, 10x/0.25 NA objective lens, and 300 lines/mm grating. The 100 nM concentration was detected with a 200 μm pinhole. The Raman spectra used for the enhancement factor calculations were collected using a Thermo Scientific DXR Raman confocal microscope, with a 780 nm/24 mW diode laser, 50 μm slit, 2.5 sec integration time with 60 exposures, 50x/0.5 NA/1.6 μm spot size long working distance objective, and 830 lines/mm grating. The spectra were collected using the Omnic Dispersive software, which subtracts the background of each signal after collection.

4.3 Results and Discussion

4.3.1 Trapping and Aggregation Test

The trapping efficiency of 1 μm PS microparticles by the silica nanofiber membrane integrated microfluidic device was investigated. The average diameter of the silica nanofibers used in this experiment was 100 nm, and the thickness of the silica nanofiber membrane was estimated in the same order of magnitude from the SEM image. Bright field microscope images of the trapping of PS microparticles are shown as a function of time in Figure 23. After PS particle solution was dispensed and vacuumed, PS particles were visibly trapped and aggregated within 1 minute at the junction of the silica nanofiber membrane and the inlet microfluidic channel. More PS microparticles

were trapped and accumulated along the channel as time progressed. During the total 100 minute observation, no additional aggregation was found outside the channel boundary, which suggested the nanopores at the junction had successfully block the larger PS microparticles.

The aggregation pattern of gold nanoparticles (Figure 24) followed the result of PS microparticles. The gold nanoparticles were found to accumulate at the end of channel in less than 30 seconds. Some of gold nanoparticles at the end of channels were aggregated outside of microfluidic channels, it is possibly because the pressure drop between two channels was initially high and some nanoparticles were migrated into silica nanofiber membranes, and then stopped by dense nanofibers at the vicinity of channel ends. Most aggregation of the gold nanoparticles aggregation still occured at the channel end, the junction of the membrane and the channel.

4.3.2 SERS Signal of Adenine

The SERS signals of different concentrations of adenine are shown in Figure 25. The areas of aggregation for the four concentrations were at the end of the inlet microchannel with a less than 10 μm sensing area. The signal intensity shows concentration dependence at 735 cm^{-1}. However, further investigation is necessary to improve the ability to obtain quantitative information and determine the ultimate limits of detection. This silica nanofiber integrated microfluidic device could be used to sense a signal down to 100 nM without optimization of Raman instrumentation parameters.

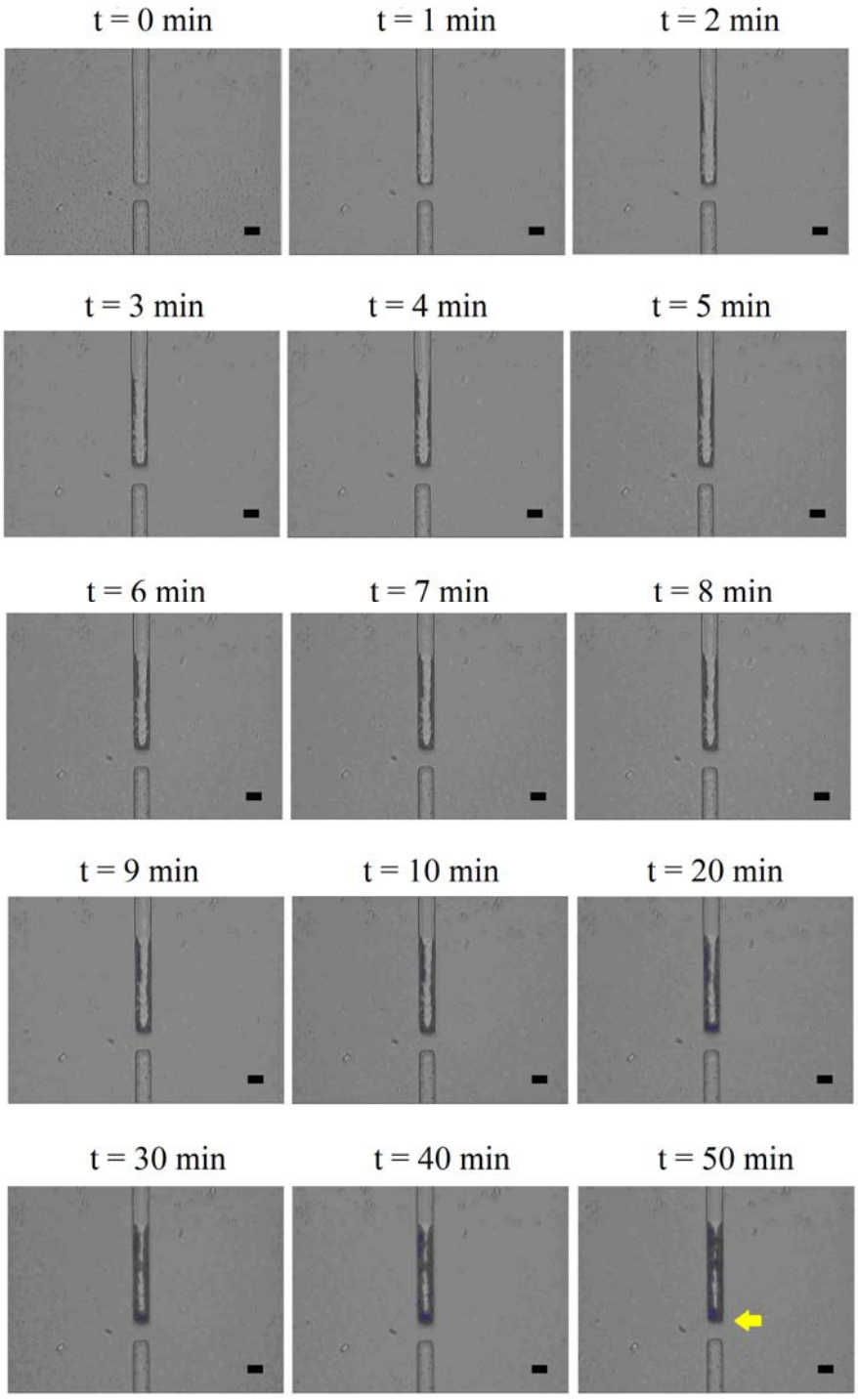

Figure 23. Bright field microscope images of the trapping of PS microparticles at the junction of the inlet microchannel and nanofiber coated channel (yellow arrow). These images show that nanopores created at the junction encourage aggregation of the microparticles. The scale bar is 20 μm.

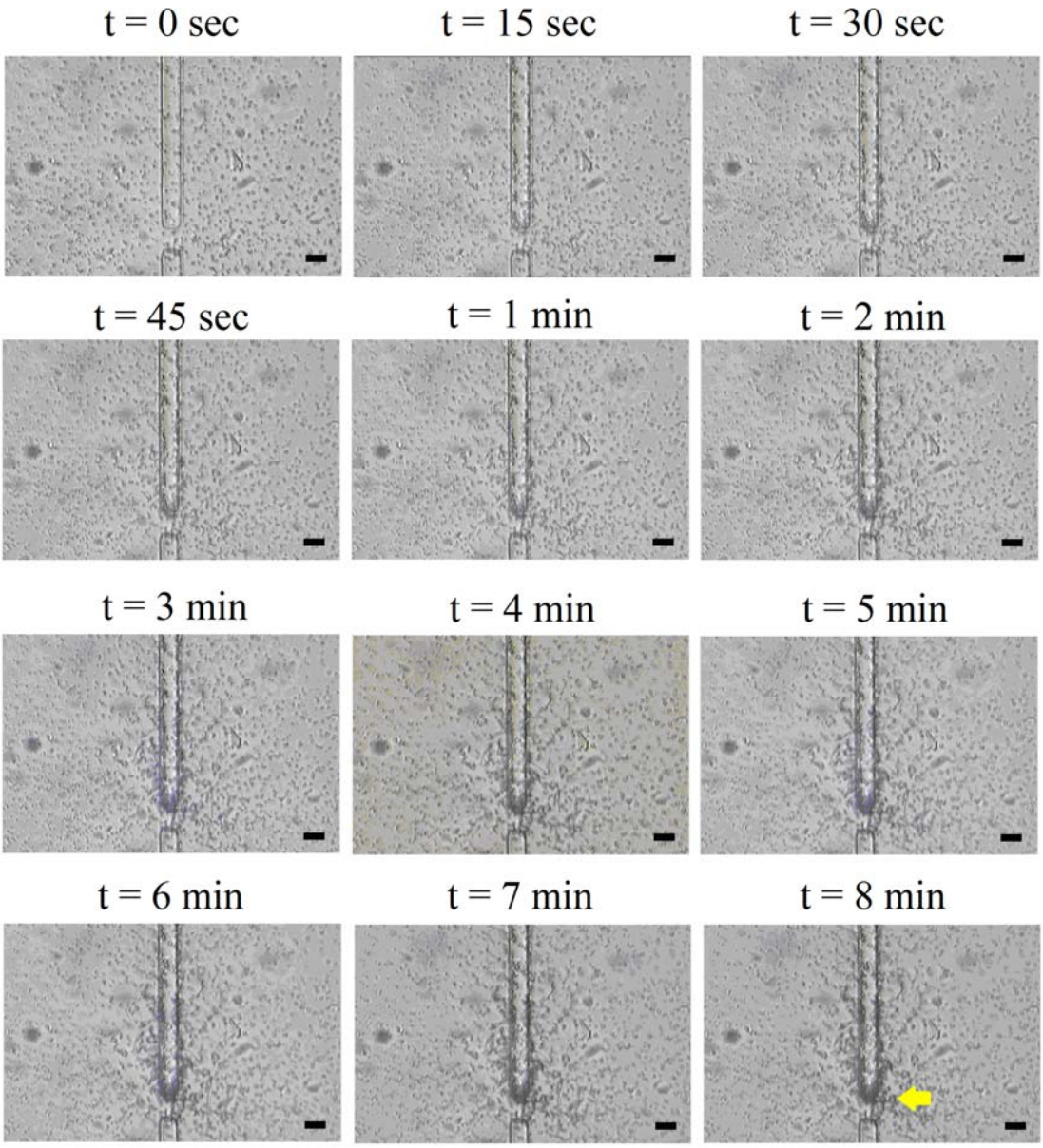

Figure 24. Bright field images of gold nanoparticle aggregation at the junction of the inlet microchannel and nanofiber coated channel (yellow arrow). Most of the aggregation was concentrated at the 25 μm bridged region since the fluidic resistance is the lowest. The scale bar is 20 μm.

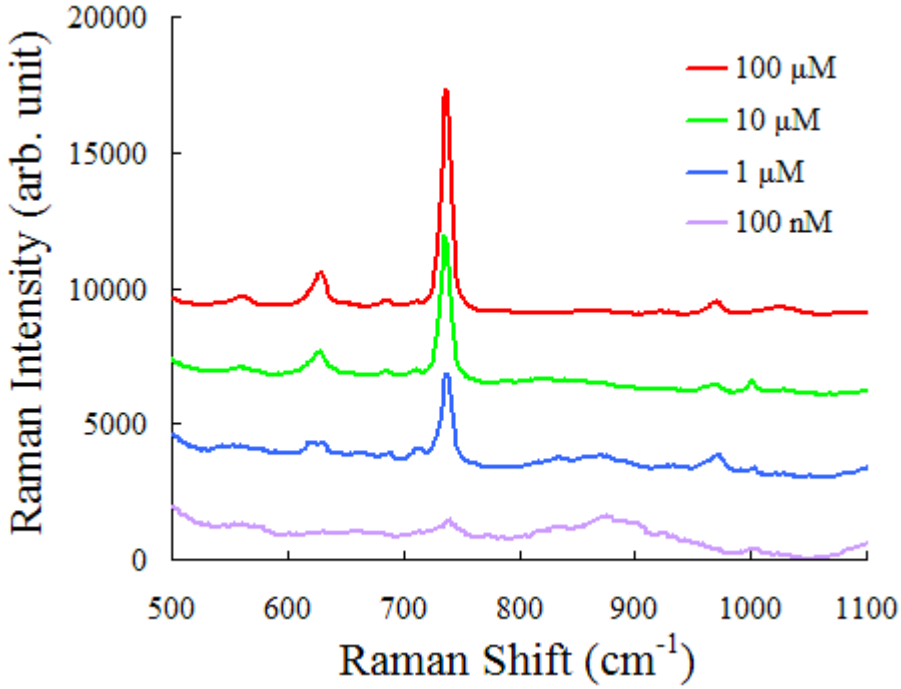

Figure 25. The SERS signals of different concentrations of adenine at aggregation spots. The 100 nM SERS signal of adenine was acquired using a 200 µm pinhole. Spectra are offset for clarity.

The time-dependent signal variation of 100 μM of adenine solution was studied after dispensing 10 μl of adenine/gold solution (9% v/v) into the reservoir of the device. SERS spectra were acquired at the end of the inlet microfluidic channel where aggregations occurred. The SERS spectra as a function of time are shown in Figure 26. No SERS signal of adenine was found at 735 cm^{-1} at the beginning of the experiment, since the surface of PDMS microfluidic channel was hydrophobic and did not allow capillary flows. After 8 minutes of vacuuming, the SERS signal of adenine gradually formed and intensified over time, saturating after 130 minutes. This result indicates that nanoparticles and adenine molecules were continuously trapped at the junction between the inlet microfluidic channel and nanofiber membrane, and reach a stability level. Although it took 8 minutes before initial detection and 130 minutes before stabilization, this flow rate can be significantly enhanced in future versions of the device by surface-modifying the hydrophobic PDMS channel to be hydrophilic and transporting the liquid using electroosmotic flow.[42-43,141-142]

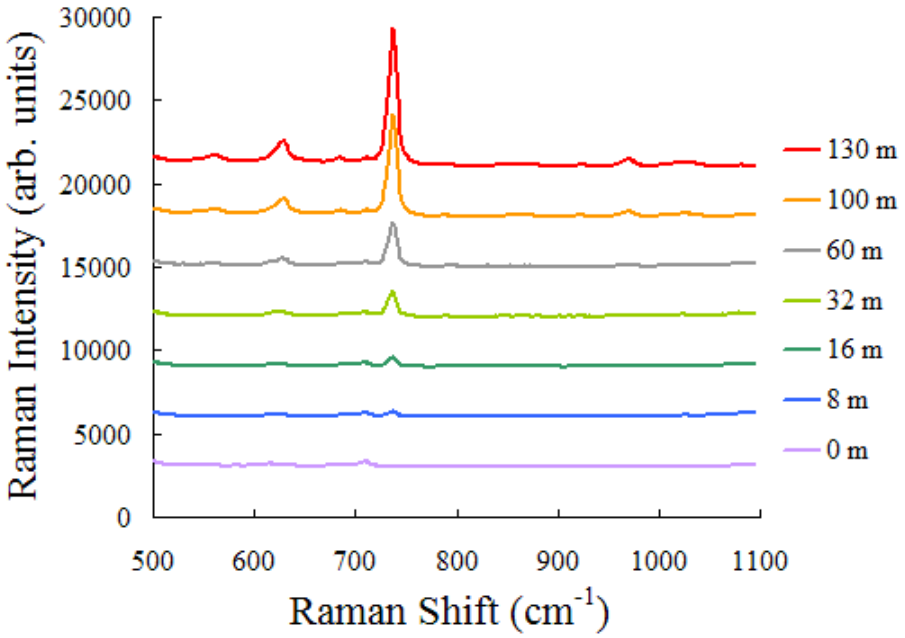

Figure 26. SERS signals of 100 µM of adenine obtained by the device at the junction between the inlet microfluidic channel and the silica nanofiber membrane as a function of time. Spectra are offset for clarity.

4.3.3 SERS Enhancement Factor

Figure 27 shows the enhancement of Raman intensity at the aggregation spot of the device compared to the intensity of 1M adenine without using gold colloid. SERS enhancement factor was calculated by comparing the SERS and Raman signal of adenine at the 735 cm^{-1} mode. The analytical enhancement factor (AEF) gives a good estimate of the average enhancement factor of the substrate. The normal Raman spectra was obtained under the same conditions as the SERS spectra and an AEF of up to 10^9 was determined using the following equation:[136]

$$AEF = (I_{SERS} / conc_{SERS}) / (I_{RS} / conc_{RS})$$

Where I_{SERS} is the intensity of the enhanced Raman signal at the concentration ($conc_{SERS}$), which is 1 µl of 1 µM adenine added to the 10 µl stock gold colloid and dispensed into the nanofiber membrane integrated microfluidic device. I_{RS} is the intensity of the non-SERS Raman measurement at the measured concentration ($conc_{RS}$), which is 300 µl of 1 M adenine without using gold colloid. This enhancement factor could be improved by the design of microfluidic channel, the optimization of the diameter and density of the electrospun nanofiber, and optimization of Raman instrumentation parameters.

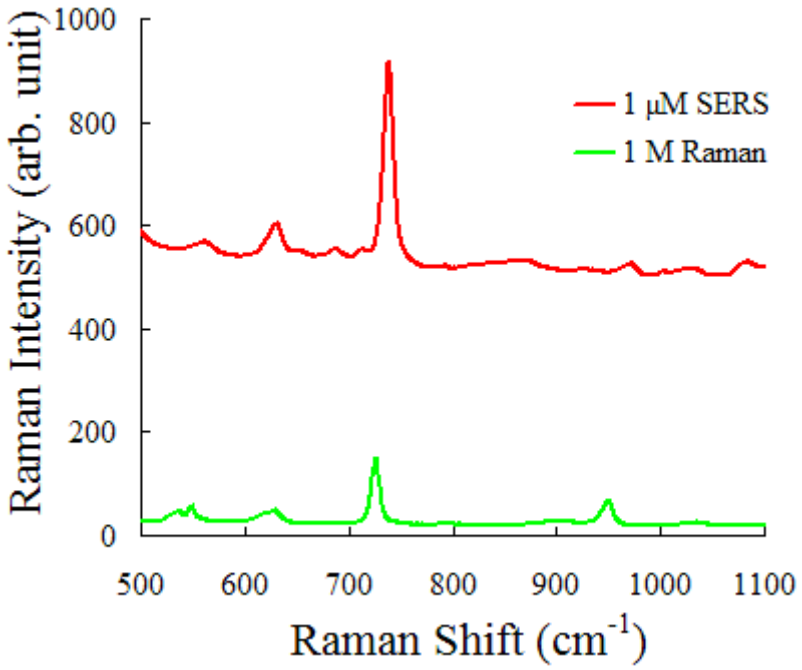

Figure 27. The SERS signal of 1µM adenine at the aggregation spot and the Raman signal of 1M adenine without using gold colloid. Spectra are offset for clarity.

4.4 Summary

We have developed a new optofluidic device that was integrated with a silica nanofiber membrane. This device has nanometer scale entrances at the boundary between a silica nanofiber membrane and the inlet microfluidic channel, where gold nanoparticles and analyte were aggregated. The device was tested with adenine and could be used to detect SERS signal down to nanomolar concentrations with a SERS enhancement factor of 10^9 without optimization. This device enables the localization of SERS hotspots. Target molecules can be guided to the desired spots instead of being absorbed randomly. The substrate can be fabricated consistently with a simple, low cost, and widely available methodology: soft-lithography and electrospinning. Once optimized, these characteristics may show potential for this approach to be used as a robust SERS and POC device.

5. SUMMARY

In this dissertation, three porous membrane-base devices for biological detection are demonstrated. These devices share the same features of low cost, high sensitivity, rapidity, portability, and the ability to improve traditional detection methods, fulfilling some of the requirements for POC test devices. The electrospun silica nanofiber membranes played important roles in the filter devices for both ELISA and SERS detection. In the case of the immunosorbent assay device, the high surface-to-volume ratio feature of electrospun silica nanofiber membrane was exploited to increase the detection area and decrease the waste of reagents, showing better detection limit down to picomolar range and good linearity of fluorescence intensity and concentration of target protein. The hybridization time was reduced from 1 day of conventional ELISA to less than 1 hour with improved sensitivity. In the case of the SERS detection device, the small surface roughness of the depositied electrospun silica nanofibers membrane on a glass slide was utilized to create nanopores after the glass slide was bonded with a PDMS microchannel layer. The SERS hotspots were confined near the junction between the inlet channel and the membrane instead of randomly distributed. The significant enhancement factor 10^9 and the nanomolar detection limit show potential of this detection device once fully optimized. The AAO membrane is the key element of the filter device for the bacteria viability detection. The features of uniform pore size, dense pore distribution, vertical pore alignment, stiffness, and nonreactive surface of this inorganic membrane are advantages over several commonly-used polymeric membranes.

The bacteria were therefore observed in a more stable situation, without the concerns of autofluorescence, deformation, fouling, and other unwanted incidents that lead to miscalculation of the cell count. The antibiotic efficacy was measured in the filter-device incorporating AAO membrane. MIC was able to be determined from 1-2 days of traditional methods to 1 hour using this AAO membrane device, showing the potential in clinical uses to reduce occurrence of microbial antibiotic resistance.

Since these membrane-based devices were only prototypes developed in academia without optimization, their future forms may be quite different from the current ones. For example, the electrospun membrane filter device for biomolecular detection can complement low concentration range, which makes it ideal to determine minute amount of target molecule after a traditional ELISA is performed but unable to sense any signal. The next version of the device may appear in the form of a membrane-based microcentrifuge tube that is highly compatible with lab equipments. For the microfluidic/electrospun membrane optofluidic device for SERS that also utilizes electrospun membrane, the device may have several inlet channels on a membrane, forming multiple junctions in between to increase the flow rate, and have a pre-filter to avoid fouling of contaminant. The AAO membrane filter device for bacteria viability detection may be the first one to be applied to POC tests, since it is established on several commercialized products and in vitro clinical tests have been conducted. In brief, a complete optimization for these membrane-based devices discussed in this dissertation should make them more suitable for real POC applications, contributing the development of rapid, accurate, reliable, and early diagnosis of patients.

REFERENCES

1. A. J. Tüdős, G. A. J. Besselink and R. B. M. Schasfoort, *Lab Chip*, 2001, **1**, 83.
2. K. Lewandrowski, *Clin. Lab. Med.*, 2009, **29**, 421.
3. S. L. Gutierres and T. E. Welty, *Ann. Pharmacother.*, 2004, **38**, 119.
4. S. C. Terry, J. H. Jerman and J. B. Angell, *Ieee T. Electron. Dev.*, 1979, **26**, 1880.
5. Agilent Technologies Inc., USA (www.agilent.com).
6. R. Suriano, A. Kuznetsov, S. M. Eaton, R. Kiyan, G. Cerullo, R. Osellame, B. N. Chichkov, M. Levi and S. Turri, *Appl. Surf. Sci.*, 2011, **257**, 6243.
7. X. Zhao and Y. C. Shin, *Appl. Phys. A*, 2011, **104**, 713.
8. M. Abonnenc, A.-L. Gassner, J. Morandini, J. Josserand and H. H. Girault, Anal. *Bioanal. Chem.*, 2009, **395**, 747.
9. A. Stojanovic, G. R. J. Artus and S. Seeger, *Nano Res.*, 2010, **3**, 889.
10. P. S. Nunes, P. D. Ohlsson, O. Ordeig and J. P. Kutter, *Microfluid. Nanofluid.*, 2010, **9**, 145.
11. M. J. Mescher, E. E. Leary Swan, J. Fiering, M. E. Holmboe, W. F. Sewell, S. G. Kujawa, M. J. McKenna and J. T. Borenstein, *J. Microelectromech. S.*, 2009, **18**, 501.
12. M. E. Wilson, N. Kota, Y. Kim, Y. Wang, D. B. Stolz, P R. LeDuc and O. B. Ozdoganlar, *Lab Chip*, 2011, **11**, 1550.
13. J. C. McDonald, D. C. Duffy, J. R. Anderson, D. T. Chiu, H. Wu, O. J. Schueller and G. M. Whitesides, *Electrophoresis*, 2000, **21**, 27.

14. J. M. Sidorova, N. Li, D. C. Schwartz, A. Folch and R. J. Monnat, *Nat. Protoc.*, 2009, **4**, 849.

15. A. O. Ogunniyi, C. M. Story, E. Papa, E. Guillen and J. C. Love, *Nat. Protoc.*, 2009, **4**, 767.

16. A. L. Paguirigan and D. J. Beebe, *Nat. Protoc.*, 2007, **2**, 1782.

17. W. Browne, M. J. Rust, W. Jung, S. H. Lee and C. H. Ahn, *Lab Chip*, 2009, **9**, 2941.

18. S.-H. Yoon, N.-G. Cha, J. S. Lee, J.-G. Park, D. J. Carter, J. L. Mead and C. M.F. Barry, *Polym. Eng. Sci.*, 2010, **50**, 411.

19. A. Griffiths, S. Bigot, E. Brousseau, M. Worgull, M. Heckele, J. Nestler and J. Auerswald, *Int. J. Adv. Manuf. Tech.*, 2010, **47**, 111.

20. U. M. Attia, S. Marson and J. R. Alcock, *Microfluid. Nanofluid.*, 2009, **7**, 1.

21. A. Mathur, S.S. Roy, M. Tweedie, S. Mukhopadhyay, S. K. Mitra and J. A. McLaughlin, *Curr. Appl. Phys.*, 2009, **9**, 1199.

22. L. P. Yeo, S. H. Ng, Z. F. Wang, H. M. Xia, Z. P. Wang, V. S0 Thang, Z. W0 Zhong and N. F. de Rooij, *J. Micromech. Microeng.*, 2010, **20**, 015017.

23. E. W. K. Young, E. Berthier, D. J. Guckenberger, E. Sackmann, C. Lamers, I. Meyvantsson, A. Huttenlocher and D. J. Beebe, *Anal. Chem.*, 2011, **83**, 1408.

24. S. Giselbrecht, T. Gietzelt, E. Gottwald, C. Trautmann, R. Truckenmüller, K. F. Weibezahn and A. Welle, *Biomed. Microdevices*, 2006, **8**, 191.

25. E. Roy, M. Geissler, J.-C. Galas and T. Veres, *Microfluid. Nanofluid.*, 2011, **11**, 235.

26. R. Truckenmüller, S. Giselbrecht, N. Rivron, E. Gottwald, V. Saile, A. van den Berg, M. Wessling and C. van Blitterswijk, *Adv. Mater.*, 2011, **23**, 1311.

27. E. Roy, J.-C. Galas and T. Veres, *Lab Chip*, 2011, **11**, 3193.

28. D. Mark, S. Haeberle, G. Roth, F. von Stetten and R. Zengerle, *Chem. Soc. Rev.*, 2010, **39**, 1153.

29. M. Wang, N. Jing, I.-H. Chou, G. L. Cote and J. Kameoka, *Lab Chip*, 2007, **7**, 630.

30. G. A. Posthuma-Trumpie, J. Korf and A. van Amerongen, *Anal. Bioanal. Chem.*, 2009, **393**, 569.

31. R. Krska and A. Molinelli, *Anal. Bioanal. Chem.*, 2009, **393**, 67.

32. H. L. Xie, W. Ma, L. Q. Liu, W. Chen, C. F. Peng, C. L. Xu and L. B. Wang, *Anal. Chim. Acta*, 2009, **634**, 129.

33. M. A. Unger, H. P. Chou, T. Thorsen, A. Scherer and S. R. Quake, *Science*, 2000, **288**, 113.

34. T. Thorsen, S. J. Maerkl and S. R. Quake, *Science*, 2002, **298**, 580.

35. S. Haeberle and R. Zengerle, *Lab Chip*, 2007, **7**, 1094.

36. S. R. Quake and A. Scherer, *Science*, 2000, **290**, 1536.

37. N. G. Anderson, *Science*, 1969, **166**, 317.

38. M. Madou, J. Zoval, G. Y. Jia, H. Kido, J. Kim and N. Kim, *Annu. Rev. Biomed. Eng.*, 2006, **8**, 601.

39. D. D. Nolte, *Rev. Sci. Instrum.*, 2009, **80**, 101101.

40. B. S. Lee, J. N. Lee, J. M. Park, J. G. Lee, S. Kim, Y. K. Cho and C. Ko, *Lab Chip*, 2009, **9**, 1548.

41. Y. K. Cho, J. G. Lee, J. M. Park, B. S. Lee, Y. Lee and C. Ko, *Lab Chip*, 2007, **7**, 565.

42. C.-K. Chou, N. Jing, H. Yamaguchi, P.-H. Tsou, H.-H. Lee, C.-T. Chen, Y.-N. Wang, S. Hong, C. Su, J. Kameoka and M.-C. Hung, *Lab Chip*, 2010, **10**, 1793.

43. C.-K. Chou, N. Jing, H. Yamaguchi, P.-H. Tsou, H.-H. Lee, C.-T. Chen, Y.-N. Wang, S. Hong, C. Su, J. Kameoka and M.-C. Hung, *Analyst*, 2010, **135**, 2907.

44. J. Lee, H. Moon, J. Fowler, T. Schoellhammer and C. J. Kim, *Sens. Actuators, A*, 2002, **95**, 259.

45. M. G. Pollack, R. B. Fair and A. D. Shenderov, *Appl. Phys. Lett.*, 2000, **77**, 1725.

46. A. Wixforth, *Superlattice. Microstruct.*, 2003, **33**, 389.

47. A. Wixforth, C. Strobl, C. Gauer, A. Toegl, J. Scriba and Z. von Guttenberg, *Anal. Bioanal. Chem.*, 2004, **379**, 982.

48. D. Beyssen, L. Le Brizoual, O. Elmazria and P. Alnot, *Sens. Actuators, B*, 2006, **118**, 380.

49. Z. Guttenberg, H. Muller, H. Habermuller, A. Geisbauer, J. Pipper, J. Felbel, M. Kielpinski, J. Scriba and A. Wixforth, *Lab Chip*, 2005, **5**, 308.

50. M. V. Kakade, S. Givens, K. Gardner, K. H. Lee, D. B. Chase and J. F. Rabolt, *J. Am. Chem. Soc.*, 2007, **129**, 2777-2782.

51. J. P. Chen, G. Y. Chang and J. K. Chen, *Colloid. Surface. A*, 2006, **313**, 183-188.

52. R. R. Klossner, H. A. Queen, A. J. Coughlin and W. E. Krause, *Biomacromolecules*, 2008, **9**, 2947-2953.

53. Y. Wang and Y. L. Hsieh, *J. Membr. Sci.*, 2008, **309**, 73-81.

54. D. Yang, Y. Jin, Y. Zhou, G. Ma, X. Chen, F. Lu and J. Nie, *Macromol. Biosci.*, 2008, **8**, 239-246.

55. M. S. Peresin, Y. Habibi, J. O. Zoppe, J. J. Pawlak and O. J. Rojas, *Biomacromolecules*, 2010, **11**, 674-681.

56. J. J.Stankus, L. Soletti, K. Fujimoto, Y. Hong, D. A. Vorp and W. R. Wagner, *Biomaterials*, 2007, **28**, 2738-2746.

57. E.-R. Kenawy, F. I. Abdel-Hay, M. H. El-Newehy and G. E. Wnek, *Mater. Chem. Phys.*, 2009, **113**, 296-302.

58. C. Yao, X. Li, K. G. Neoh, Z. Shi and E. T. Kang, *J. Membrane. Sci.*, 2008, **320**, 259-267.

59. T. Uyar, I. Cianga, L. Cianga, F. Besenbacher and Y. Yagci, *Mater. Lett.*, 2009, **63**, 1638-1641.

60. S. I. Jeong, I. D. Jun, M. J. Choi, Y. C. Nho, Y. M. Lee and H. Shin, *Macromol. Biosci.*, 2008, **8**, 627-637.

61. N. J. Pinto, I. Ramos, R. Rojas, P.-C. Wang and A. T. Johnson, *Sensor. Actuat. B-Chem.*, 2008, **129**, 621-627.

62. D. H. Reneker and A. L. Yarin, Polymer, 2008, **49**, 2387-2425.

63. N. Bhardwaj and S. C. Kundu, *Biotechnol. Adv.*, 2010, **28**, 325-347.

64. S. Sahoo, S. L. Toh and J. C. H. Goh, Biomaterials, 2010, **31**, 2990-2998.

65. Y. Dzenis, *Science*, 2004, **304**, 1917-1919.

66. X. Wang, C. Drew, S. H. Lee, K. J. Senecal, J. Kumar and L. A. Samuelson, *Nano Lett.*, 2002, **2**, 1273-1275.

67. H. Yoshimotoa, Y. M. Shina, H. Teraia and J. P. Vacantia, *Biomaterials*, 2003, **24**, 2077-2082.

68. Y. Zhou, M. Freitag,J. Hone, C. Staii and A. T. Johnson, Jr., *Appl. Phys. Lett.*, 2003, **83**, 3800-3802.

69. T. J. Sill and H. A. von Recum, *Biomaterials*, 2008, **29**, 1989-2006.

70. S. Agarwal, J. H. Wendorff and A. Greiner, *Polymer*, 2008, **49**, 5603-5621.

71. V. Thavasi, G. Singh and S. Ramakrishna, *Energ. Environ. Sci.*, 2008, **1**, 205-221.

72. S. Barth, F. Hernandez-Ramirez, J. D. Holmes and A. Romano-Rodriguez, *Prog. Mater. Sci.*, 2010, **55**, 563-627.

73. M. J. Duffy, *Clin. Chem.*, 2006, **52**, 345-351.

74. M. H. Kollef, *Respir. Care.*, 2005, **50**, 714.

75. M. H. Kollef, L. E. Morrow, M. S. Niederman, K. V. Leeper, A. Anzueto, L. Benz-Scott and F. J. Rodino, *Chest*, 2006, **129**, 1210.

76. M. H. Kollef and S. Ward, *Chest*, 1998, **113**, 412.

77. P. J. Z. Teixeira, R. Seligman, F. T. Hertz, D. B. Cruz and J. M. G. Fachel, *J. Hosp. Infect*., 2007, **65**, 361.

78. A. W. Bauer, W. M. Kirby, J. C. Sherris and M. Turck, *Am. J. Clin. Pathol*., 1966, **45**, 493.

79. H. F. Charnbers, *Clin. Microbiol. Rev*., 1997, **10**, 781.

80. M. B. Huang, C. N. Baker, S. Banerjee and F. C. Tenover, *J Clin Microbiol*., 1992, **30**, 3243.

81. L. K. McDougal, C. Thornsberry, *J. Clin. Microbiol*., 1986, **23**, 832.

82. C. Thornsberry and L. K. McDougal, *J. Clin. Microbiol*., 1983, **18**, 1084.

83. S. Unal, K. Werner, P. DeGirolami, F. Barsanti and G. Eliopoulos, *Antimicrob. Agents Chemother*., 1994, **38**, 345.

84. G. L. Woods, G. S. Hall, I. Rutherford, K. J. Pratt and C. C. Knapp, *J. Clin. Microbiol*., 1986, **24**, 349–352.

85. M. K. York, L. Gibbs, F. Chehab and G. F. Brooks, *J. Clin. Microbiol*., 1996, **34**, 249.

86. M. H. Kollef and S. Ward, *Chest*, 1998, **113**, 412.

87. R. H. Perry and D. H. Green, *Perry's Chemical Engineers' Handbook*, 7th edition, McGraw-Hill, 1997, 22-40.

88. http://http://en.wikipedia.org/wiki/Synthetic_membrane

89. http://www.whatman.com/products.aspx?PID=193

90. H. Masuda, K. Yada and A. Osaka, *Jpn. J. Appl. Phys.*, 1998, **37**, L1340-L1342.

91. P. Forrer, F. Schlottig, H. Siegenthaler and M. Textor, *J. Appl. Electrochem.*, 2000, **30**, 533-541.

92. A. P. Goodey, S. M. Eichfeld, K. K. Lew, J. M. Redwing and T. E. Mallouk, *J. Am. Chem. Soc.*, 2007, **129**, 12344-12345.

93. J. K. Lee, W. K. Koh, W. S. Chae and Y. R. Kim, *Chem. Commun.*, 2002, **2**, 138-139.

94. J. Oh, Y. Tak and Y. Lee, *Electrochem. Solid-State Lett.*, 2004, **7**, C27-C30.

95. J. G. Wang, M. L. Tian, N. Kumar and T. E. Mallouk, *Nano Lett.*, 2005, **5**, 1247-1253.

96. S. Zhao, H. Roberge, A. Yelon and T. Veres, *J. Am. Chem. Soc.*, 2006, **128**, 12352-12353.

97. F. Qu, M. Yang, G. Shen and R. Yu, *Biosens. Bioelectron.*, 2007, **22**, 1749-1755.

98. D. Li, R. S. Thompson, G. Bergmann and J. G. Lu, *Adv. Mater.*, 2008, **20**, 4575-4578.

99. M. D. Dickey, E. A. Weiss, E. J. Smythe, R. C. Chiechi, F. Capasso and G. M. Whitesides, *ACS Nano*, 2008, **2**, 800-808.

100. X. Gao, L. Liu, B. Birajdar, M. Ziese, W. Lee, M. Alexe and D. Hesse, *Adv. Funct. Mater.*, 2009, **19**, 3450-3455.

101. V. Haehnel, S. Fahler, P. Schaaf, M. Miglierini, C. Mickel, L. Schultz and H. Schlorb, *Acta Mater.*, 2010, **58**, 2330-2337.

102. H. C. Hesse, D. Lembke, L. Dossel, X. Feng, K. Mullen and L. Schmidt-Mende, *Nanotechnology*, 2011, **22**, 055303.

103. P. Ciambelli, L. Arurault, M. Sarno, S. Fontorbes, C. Leone, L. Datas, D. Sannino, P. Lenormand and S. L. Du Plouy, *Nanotechnology*, **22**, 265613.

104. J.-M. Moon, D. Akin, Y. Xuan, P. D. Ye, P. Guo and R. Bashir, *Biomed. Microdevices*., 2009, **11**, 135–142.

105. H. U. Osmanbeyoglu, T. B. Hur and H. K. Kim, *J. Membr. Sci.*, 2009, **343**,1–6.

106. D. C. Kim, A.-R. Jang, D. J. Kang, *Curr. Appl. Phys.*, 2009, **9**, 1454-1458.

107. M. Fleischmann, P. J. Hendra and A. J. McQuillan, *Chem. Phys. Lett.*, 1974, **26**, 163-166.

108. P. Mandal and S. A. Ramakrishna, *Opt. Lett.*, 2011, **36**, 3705.

109. N. Mattiucci, G. D'Aguanno, H. O. Everitt, J. V. Foreman, J. M. Callahan, M. C. Buncick and M. J. Bloemer, *Opt. Express*, 2012, **20**, 1868.

110. S. M. Mahurin, J. John, M. J. Sepaniak and S. Dai, *Appl. Spectrosc.*, 2011, **65**, 417.

111. E. del Puerto, C. Domingo, S. Sanchez-Cortes, J. V. Garcia-Ramos and R. F. Aroca, *J. Phys. Chem. C*, 2011, **115**, 16838.

112. T. Y. Liao, B.-Y. Lee, C.-W. Lee and P.-K. Wei, *Sens. Actuators. B*, 2011, **156**, 245.

113. L. Wu, H. C. Li, H. F. Zhao, Y. Sun, H. R. Xu, M. Lu, C. H. Yang, W. Z. Li and Z. Q. Li, *Chinese. J. Anal. Chem.*, 2011, **39**, 1159.

114. E. Kammer, T. Dorfer, A. Csaki, E. Schumacher, P. A. Da Costa, N. Tarcea, W. Fritzsche, P. Rosch, M. Schmitt and J. Popp, *J. Phys. Chem. C*, 2012, **116**, 6083.

115. X. Dong, H. M. Gu and F. F. Liu, *Spectrochim. Acta. Part A*, 2012, **88**, 97.

116. S. Lee, J. H. Wong and S. J. Liu, *Appl. Spectrosc.*, 2011, **65**, 996.

117. H. Wang, C. S. Levin. and N. J. Halas, *J. Am. Chem. Soc.*, 2005, **127**, 14992.

118. S. K. Jha, Z. Ahmed, M. Agio, Y. Ekinci and J. F. Loffler, *J. Am. Chem. Soc.*, 2012, **134**, 1966.

119. N. Félidj, J. Aubard, G. Lévi, J. R. Krenn, M. Salerno, G. Schider, B. Lamprecht, A. Leitner, and F. R. Aussenegg, *Phys. Rev. B: Condens. Matter Mater. Phys.*, 2002, **65**, 075419-1.

120. J. Theiss, P. Pavaskar, P. M. Echternach, R. E. Muller and S. B. Cronin, *Nano Lett.*, 2010, **10**, 2749.

121. N. Félidj, J. Aubard, G. Lévi, J. R. Krenn, A. Hohenau, G. Schider, A. Leitner, and F. R. Aussenegg, *Appl. Phys. Lett.*, 2003, **82**, 3095.

122. B. Yan, A. Thubagere, W. R. Premasiri, L. D. Ziegler, L. Dal Negro and B. M. Reinhard, *ACS Nano*, 2009, **3**, 1190.

123. J. L. Abell, J. M. Garren and Y. P. Zhao, *Appl. Spectrosc.*, 2011, **65**, 734.

124. Y. J. Liu, Z. Y. Zhang, R. A. Dluhy and Y. P. Zhao, *J. Raman Spectrosc.*, 2010, **41**, 1112.

125. X. B. Du, H. Y. Chu, Y. W. Huang and Y. P. Zhao, *Appl. Spectrosc.*, 2010, **64**, 781.

126. S. Shanmukh, L. Jones, J. Driskell, Y. Zhao, R. Dluhy and R. A. Tripp, *Nano Lett.*, 2006, **6**, 2630.

127. G. V. P. Kumar, N. Rangarajan, B. Sonia, P. Deepika, N. Rohman and C. Narayana, *Bull. Mater. Sci.*, 2011, **34**, 207.

128. W. B. Li, Y. Y. Guo and P. Zhang, *J. Phys. Chem. C*, 2010, **114**, 7263.

129. J. B. Jackson, S. L. Westcott, L. R. Hirsch, J. L. West and N. J. Halas, *Appl. Phys. Lett.*, 2003, **82**, 257.

130. C. E. Talley, J. B. Jackson, C. Oubre, N. K. Grady, C. W. Hollars, S. M. Lane, T. R. Huser, P. Nordlander and N. J. Halas, *Nano Lett.*, 2005, **5**, 1569.

131. C. M. S. Izumi, M. G. Moffitt and A. G. Brolo, *J. Phys. Chem. C*, 2011, **115**, 19104.

132. S. K. Yang, W. P. Cai, L. C. Kong and Y. Lei, *Adv. Funct. Mater.*, 2010, **20**, 2527.

133. M. A. Ochsenkuhn, C. J. Campbell, *Chem. Commun.*, 2010, **46**, 2799.

134. S. W. Bishnoi, Y. J. Lin, M. Tibudan, Y. M. Huang, M. Nakaema, V. Swarup and T. A. Keiderling, *Anal. Chem.*, 2011, **83**, 4053.

135. G. Q. Liu, Y. Li, G. T. Duan, J. J. Wang, C. H. Liang and W. P. Cai, *ACS Appl. Mater. Interfaces*, 2012, **4**, 1.

136. E. C. Le Ru and P. G. Etchegoin, in *Principles of Surface-Enhanced Raman Spectroscopy*, Elsevier, Oxford, 2009, pp. 1-28.

137. K. Kneipp, Y. Wang, H. Kneipp, L. T. Perelman, I. Itzkan, R. R. Dasari and M. S. Feld, *Phys. Rev. Lett.*, 1997, **78**, 1667.

138. Y. Xia and G. M. Whitesides, *Angew. Chem., Int. Ed.*, 1998, **37**, 550.

139. S. R. Quake and A. Scherer, *Science*, 2000, **290**, 1536.

140. J. Krzaczkowska, J. Gierszewski and G. Slosarek, *J. Solution Chem.*, 2004, **33**, 395.

141. J. W. Zhou, A. V. Ellis and N. H. Voelcker, *Electrophoresis*, 2010, **31**, 2.

142. M. Li and D. P. Kim, *Lab Chip*, 2011, **11**, 1126.

VITA

Name: Pei-Hsiang Tsou

Address: Department of Electrical & Computer Engineering, Texas A&M University, College Station, TX 77843-3128

Email Address: tsou3@tamu.edu

Education: B.S., Electronics Engineering, National Chiao Tung University, Hsinchu, Taiwan, 2001

\- M.S., Electrical Engineering, Texas A&M University, 2006

Publications:

1. Pei-Hsiang Tsou, Chao-Kai Chou, Sandra M Saldana, Mien-Chie Hung and Jun Kameoka, “The fabrication and testing of electrospun silica nanofiber membranes for the detection of proteins” *Nanotechnology*, 2008, 19, 445714 doi: 10.1088/0957-4484/19/44/445714.
2. Pei-Hsiang Tsou, Harini Sreenivasappa, Sungmin Hong, Masayuki Yasuike, Hiroshi Miyamoto, Keiyo Nakano, Takeyuki Misawa, Jun Kameoka, "Rapid antibiotic efficacy screening with aluminum oxide nanoporous membrane filter-chip and optical detection system" *Biosensors and Bioelectronics*, 2010, doi:10.1016/j.bios.2010.06.034.
3. Chao-Kai Chou, Nan Jing, Hirohito Yamaguchi, Pei-Hsiang Tsou, Heng-Huan Lee, Chun-Te Chen, Ying-Nai Wang, Sungmin Hong, Chin Su, Jun Kameoka and Mien-Chie Hung, "High speed digital protein interaction analysis using microfluidic single molecule detection system" *Lab on a Chip*, 2010, 10, 1793–1798 doi:10.1039/c002937h.
4. Chao-Kai Chou, Nan Jing, Hirohito Yamaguchi, Pei-Hsiang Tsou, Heng-Huan Lee, Chun-Te Chen, Ying-Nai Wang, Sungmin Hong, Chin Su, Jun Kameoka and Mien-Chie Hung, "Rapid detection of two-protein interaction with a single fluorophore by using a microfluidic device" *Analyst*, 2010, doi:10.1039/C0AN00229A.